



The chondrocranial key: Fetal and perinatal morphogenesis of the sphenoid bone in primates

Festschrift in Honour of Professor Wolfgang Maier

Edited by Ingmar Werneburg & Irina Ruf

Nanami Mano¹, Brody Wood¹, Lanre Oladipupo¹, Rebecca Reynolds¹, Jane Taylor², Emily Durham³, James J. Cray^{2,4}, Chris Vinyard⁵, Valerie B. DeLeon⁶, Timothy D. Smith^{1*}

¹ School of Physical Therapy, Slippery Rock University, Slippery Rock, PA 16057, U.S.A.

² Department of Biomedical Education and Anatomy, The Ohio State College of Medicine, Columbus, OH 43210, U.S.A.

³ Department of Anthropology, Penn State University, State College, PA 16801, U.S.A.

⁴ Division of Biosciences, The Ohio State College of Dentistry, Columbus, OH 43210, U.S.A.

⁵ Department of Anatomy and Neurobiology, Northeast Ohio Medical University, Rootstown, OH 44272, U.S.A.

⁶ Department of Anthropology, University of Florida, Gainesville, FL 32611, U.S.A.

<http://zoobank.org/4AADD7FD-8044-46BC-9614-08CBA8124AC4>

Corresponding authors: Tim D. Smith (timothy.smith@sru.edu)

Academic editor Irina Ruf | **Received** 14 March 2021 | **Accepted** 25 June 2021 | **Published** 16 August 2021

Citation: Mano N, Wood B, Oladipupo L, Reynolds R, Taylor J, Durham E, Cray JJ, Vinyard C, DeLeon VB, Smith TD (2021) The chondrocranial key: Fetal and perinatal morphogenesis of the sphenoid bone in primates. *Vertebrate Zoology* 71: 535–558. <https://doi.org/10.3897/vz.71.e65934>

Abstract

The sphenoid bone articulates with multiple basicranial, facial, and calvarial bones, and in humans its synchondroses are known to contribute to elongation of the skull base and possibly to cranial base angulation. Its early development (embryological, early fetal) has frequently been studied in a comparative context. However, the perinatal events in morphogenesis of the sphenoid have been explored in very few primates. Using a cross-sectional age sample of non-human primates (n=39; 22 platyrrhines; 17 strepsirrhines), we used microcomputed tomographic (μ CT) and histological methods to track age changes in the sphenoid bone. In the midline, the sphenoid expands its dimensions at three growth centers, including the sphenooccipital, intrasphenoidal (ISS) and presphenoseptal (PSept) synchondroses. Bilaterally, the alisphenoid is enlarged via appositional bone growth that radiates outward from cartilaginous parts of the alisphenoid during midfetal stages. The alisphenoid remains connected to the basitrabecular process of the basisphenoid via the alibasisphenoidal synchondrosis (ABS). Reactivity to proliferating cell-nuclear antigen is observed in all synchondroses, indicating active growth perinatally. Between mid-fetal and birth ages in *Saguinus geoffroyi*, all synchondroses decrease in the breadth of proliferating columns of chondrocytes. In most primates, the ABS is greatly diminished by birth, and is likely the earliest to fuse, although at least some cartilage may remain by at least one-month of age. Unlike humans, no non-human primate in our sample exhibits perinatal fusion of ISS. A dichotomy among primates is the orientation of the ABS, which is more rostrally directed in platyrrhines. Based on fetal *Saguinus geoffroyi* specimens, the ABS was initially oriented within a horizontal plane, and redirects inferiorly during late fetal and perinatal stages. These changes occur in tandem with forward orientation of the orbits in platyrrhines, combined with downward growth of the midface. Thus, we postulate that active growth centers direct the orientation of the midface and orbit before birth.

Keywords

appositional bone, basicranial, cartilage, craniofacial, endochondral, growth center, Zuwachsknochen

Introduction

The mammalian sphenoid ossifies within the center of the chondrocranium, the cartilaginous template for most bones of the basicranium the ethmoid bone, and nasal cartilages (Starck 1967). When it first ossifies, multiple ossification centers coalesce as two midline elements, the presphenoid and basisphenoid, and paired bilateral elements, the orbitosphenoids and alisphenoids (de Beer 1937). During its development, the sphenoid bone unites all three developmental regions of the growing cranium (dermatocranium, viscerocranium, chondrocranium). With its numerous synchondroses and sutures, the sphenoid bone represents a crucial intersection within the cranium. Its contribution to the calvarium arises during early fetal development, when a membranous expansion extends from the chondrocranial root of the alisphenoid (Maier 1987; Presley 1993). As sphenoidal ossification centers emerge, cartilaginous joints persist among them and with the occipital and ethmoid bone. To the extent that these joints remain cartilaginous, these are often considered important locations of interstitial growth that expand the anteroposterior dimensions of the cranial base (Ford 1958; Scott 1958; Baume 1968; Michejda 1972; Melsen 1974), and also influence facial orientation via joints with the ethmoid bone, another derivative of the chondrocranium (Scott 1953; Baume 1968; Smith et al. 2017). Thus, many of the joints of the sphenoid bone are active “growth centers” that may affect the form of the cranium (Baume 1968; McBratney-Owen et al. 2008). However, our understanding of how and when these joints influence basicranial and overall craniofacial form are based on very few tissue-level observations. We recently studied basicranial joints in a broad array of non-human primates at birth (Smith et al. 2021a), and established that up to eight of these have characteristics indicating active growth (see below). Histological evidence across age exists for humans, a few primates, and various non-primates (e.g., Baume 1968; Hoyte 1973; Melsen 1974, 1977; Heinkele et al. 1989; Kjaer 1990).

Prior to ossification, the sphenoid itself is initially restricted to the chondrocranium, where it is directly continuous with the nasal septal cartilage of the midface (de Beer 1937). This link to the face, a region which later is predominantly housed by viscerocranial bones, persists postnatally. The sphenoid shares an interface with the ethmoid bone. The presphenoid bone may project anteriorly within the facial skeleton (Maier 1983; Smith et al. 2017).

There has been little focus on postembryonic prenatal development of the lateral parts of the sphenoid in non-human primates until recently (Smith et al. 2021a). In the present study we examine the development of the sphenoid bone in non-human primates across prenatal and early postnatal age. Our small prenatal sample is mainly used to assess mid-fetal patterns of morphogenesis of the alisphenoid and the bilateral synchondroses that unite it with the basisphenoid.

Morphogenesis of the sphenoid in humans

Development of the sphenoid is best understood in humans (Fawcett 1910; Kjaer 1990, Cunningham et al. 2016), rodents (e.g., Dai et al. 2017), and some other mammals (e.g., *Monodelphis domestica* – Maier 1987). Skull development starts after the development of other cranial structures such as the brain, cranial nerves, the eyes, and blood vessels (Sperber 2001). Regarding sphenoid bone development, chondrification centers form two hypophyseal (postsphenoid) cartilages that fuse to form the hypophyseal plate (lamina hypophyseos) in which the basisphenoid (postsphenoid) ossifies. Two trabecular cartilages fuse to form a template within which the presphenoid ossifies. Bilateral chondrification centers of the orbitosphenoid (lesser wing) and the root of the alisphenoid (greater wing) form laterally to become the wings of the sphenoid bone (Sperber 2001).

The basisphenoid ossifies prior to the presphenoid, based on fetuses of different ages (Kjaer 1990). The body of the human basisphenoid is consistently described as having four centers of ossification: paired medial centers (which may instead form as a single large midline center) and paired lateral centers (Kier and Rothman 1986; Kodama 1986b; Sasaki and Kodama 1986). The latter pair ossifies within the alar process of the ala temporalis. The presphenoid and paired orbitosphenoids have a complex pattern of ossification. Kodama (1986a) observed up to nine ossification centers in the presphenoid. The first, the bilateral centers of the body of the presphenoid, were present in one of 11 of the smallest fetuses studied (14–19 cm sitting height (SH)); these centers were present in all 12 of the largest fetuses studied (42–40 cm SH). Anterior accessory centers, found anterosuperior to the optic canal, appeared in some but not all fetuses ranging in size from 24.5 to 40 cm SH. Five additional centers were present in some but not all fetuses ranging from 31 to 40 cm SH. The observations of fewer ossification centers in larger fetuses could mean some centers appear later, or could be interpreted to mean the total number of ossification centers varies. A study of prenatal specimens prepared using whole-mount staining for bone (Kier and Rothman 1986) clearly indicates the timing of ossification of these centers may vary. The presphenoid-orbitosphenoid complex begins to form at an early fetal stage (16 weeks) in humans, with the posterior crus of the orbitosphenoid (a.k.a., inferior or metoptic root of the orbitosphenoid) fusing first to the presphenoid body. The basisphenoid centers also fuse into a single mass by about 16 weeks, but the body and paired alisphenoids remain separated throughout the remainder of gestation. The medial center of the presphenoid fuses with the anterosuperior aspect of the lesser sphenoid wing, forming the planum sphenoidale at around the first year of life (Som and Naidich 2013).

In humans, the six primary osseous parts of the sphenoid (basis- and presphenoid, alisphenoid, orbitosphenoid) form from when multiple centers of ossification

merge at early fetal ages (as early as the 3rd fetal month): the midline presphenoid and basisphenoid and paired orbitosphenoids and alisphenoids (Fawcett 1910; and see Cunningham et al. 2016). Pterygoid plates represent additional ossifications, including intramembranous bone of each plate and endochondral bone of the hamulus; by late fetal stages these fuse to the basal side of the alisphenoid to become an alisphenoid-ptyergoid complex.

As in other mammals, the human sphenoid enlarges due to active expansion at cartilaginous growth centers and the addition of appositional bone, or *Zuwachsknochen* (Maier 1987), most notably to the alisphenoid. This appositional bone expands into the anterolateral (sphenoidal) fontanelle, which is widely patent at birth (Cunningham et al. 2016). Also at birth, synchondroseal expansion continues; this is the major focus of the present study.

The role of synchondroses in sphenoid ontogeny

Interstitial growth, that is, growth by cellular mitosis and matrix production within an already existing tissue mass, is a key feature distinguishing cartilage from bone (Hunziker 1994). Both bone and cartilage grow appositionally, that is, at the edges of already chondrified/ossified tissue. But cartilage can grow directionally by virtue of organized rows of proliferating and hypertrophic chondrocytes (Hunziker 1994). Such is the organization of epiphyseal growth plates and basicranial synchondroses (e.g., Yoon et al. 2019). Increased chondrocyte numbers, chondrocyte size, and matrix production are all factors that drive tissue expansion in synchondroses, and for this reason, these specialized cartilaginous joints are called “growth centers” (Baume 1968). This presents a contrast to cranial sutures, which remain patent during growth, and are thus considered passive “growth sites” that allow soft organs or developing teeth to increase in dimensions.

Midline synchondroses of the cranial base are considered important growth centers for skull development, and premature cessation of growth at these joints has far-reaching impacts on both neurocranial and facial form (e.g., Krieborg et al. 1993). Within the sphenoid, there are at least two midline synchondroses, the sphenoccipital synchondrosis (SOS; between basioccipital and basisphenoid) and the intrasphenoidal synchondrosis (ISS, between the basi- and presphenoid). A third joint, the sphenothmoidal synchondrosis (SES), may intervene between the developing presphenoid and ethmoid; however, its tissue composition may vary among mammals (Smith et al. 2021a). Tissue level studies are required to discern the characteristics that denote growth within synchondroses, and these are well studied in rodent animal models (e.g., Durham et al. 2017; Yoon et al. 2019). Few histological studies of primates have been done. A study by Thilander and Ingervall (1973) employed a human sample spanning ages from birth to 24 years, but there is very little similar work on nonhuman primates. One exception is the

study by Michejda (1972) on an age-range of subadult macaques (*Macaca mulatta*). Additionally, Heinkele et al. (1989) studied a sample of green monkeys (*Cercopithecus aethiops*), but this work examined a far shorter age range in terms of growth (mixed dentition to late adulthood). Both of these studies focused on the SOS, the most studied of basicranial growth centers. It is present for the most prolonged postnatal interval of all the midline synchondroses in humans, completely fusing between 16–20 years (Som and Naidich 2013; Cendekiawan et al. 2010; Cunningham et al. 2016; Dai et al. 2017), although cessation of cartilage growth is earlier (Thilander and Ingervall 1973).

Other sphenoidal synchondroses have received far less focus. The ISS is active prenatally, but is understood to fuse perinatally in humans. Baume (1968) observed ISS as an isolated remnant in a human newborn, which had already begun to fuse. Shopfner et al. (1968) provided histology of the sphenoid in a two week old infant, and attempted to indicate the ISS, although artifactual damage renders this rather uncertain. However, they also photographed a gross midsagittally cut sphenoid of a 30 week-old stillborn, in which the ISS is plainly present, showing separated pre- and basisphenoid ossification centers. Shopfner et al. (1968) also provide radiographic evidence of a cleft at the location of ISS, which is present in most (~65%) infants up to one-month of age, less than half of older infants up to two years, and only 3% of 3-year-olds. These data are highly suggestive of synchondroseal fusion, and indicate that the ISS may begin to fuse immediately before birth or during early infancy.

In reviews and texts, the SES is widely reported to remain patent in humans until ~ 6 years of age (Lieberman et al. 2000; Sperber 2001; Cunningham et al. 2016; Lesciotta and Richtsmeier 2019). However, the ontogeny of this joint is more difficult to study based on its small size. It is difficult to resolve even using many modern imaging techniques (Jeffrey and Spoor 2002), and it has rarely been studied in humans using histology. Baume (1968) did examine SES at different prenatal stages and at birth, and revealed this site becomes a fibrous joint (i.e., collagenous and non-cartilaginous) at birth in humans (hence he prefers “suture”), in contrast to rats (in which it is an active cartilaginous growth center). Recently, we demonstrated a fibrous SES is also seen in at least several species of Old and New World monkeys at birth (e.g., *Papio anubis*, *Saguinus oedipus*; Smith et al. 2021a). In strepsirrhines, cartilage at this joint persists at birth, but it is not organized into proliferating and hypertrophic chondrocyte zones (Smith et al. 2021a). Thus, SES may contribute quite differently to basicranial growth than other midline synchondroses. At least in anthropoids, it may function as a passive growth site postnatally, and thus the term sphenothmoidal *suture* has been used by some (Baume 1968; Cendekiawan et al. 2010).

The presphenoid articulates with the septal cartilage in the midline, ventral to SES, at the presphenoseptal synchondrosis (PSept). Our recent histological study revealed the PSept is a cartilaginous growth center at birth in an entire sample of strepsirrhines and monkeys (Smith

Table 1. Sample size, ages and stages, and source of specimens studied

Species	n	Age range	source
Suborder Haplorhini Infraorder Platyrrhini			
<i>Saguinus geoffroyi</i>	3	Fetal (2), newborn	Cleveland Metroparks Zoo, Cleveland, OH, U.S.A.
<i>Saguinus oedipus</i>	9	late fetal (1); newborn (7); one-month-old (1)	New England Primate Research Center, Cambridge, MA, U.S.A.
<i>Saimiri boliviensis</i>	10	late fetal (2), newborn (8)	Michale E. Keeling Center for Comparative Medicine and Research, Bastrop, TX, U.S.A.
Suborder, Strepsirrhini			
<i>Lemur catta</i>	6	late fetal (2); newborn (2); infant (2*)	Duke Lemur Center, Durham, NC, U.S.A.
<i>Varecia</i> spp. (<i>V. rubra</i> , <i>V. variegata</i>)	4	late fetal (1, <i>V. rubra</i>), newborn (1 <i>V. rubra</i> , 1 <i>V. variegata</i>), infant (1, <i>V. variegata</i>)	Duke Lemur Center, Durham, NC, U.S.A.
<i>Otolemur crassicaudatus</i>	4	late fetal (2), newborn (1), ~ one-month-old (1)	Duke Lemur Center, Durham, NC, U.S.A.
<i>Loris tardigradus</i>	2	midgestation	Duke Lemur Center, Durham, NC, U.S.A.
<i>Nycticebus coucang</i> (Hubrecht specimen # 36)	1	early fetal	Hubrecht collection, Museum für Naturkunde, Berlin, Germany

*, one infant *L. catta* had a recorded postnatal age of 28 days, a second infant 19 days of age; both were similar in status of dental eruption.

et al. 2017). In contrast, there is no evidence of cartilaginous growth in perinatal or older infant humans. Instead, histological observations suggest that the cartilage at the leading edge of the sphenoid, which continues into the nasal septum, degenerates perinatally (Baume 1968; Melsen 1974). Baume (1968, p. 506) described the site of PSept to be in a state of “desmolytic degeneration” in a newborn. Thus, its growth capacity is likely akin to a suture (i.e., passive) in humans during infancy.

A final sphenoidal synchondrosis is found bilaterally between the midline basisphenoid and alisphenoids, the alibasisphenoidal synchondrosis (ABS – Smith et al. 2021a). Because these basisphenoids and alisphenoid fuse during the first postnatal year in humans (Cunningham et al. 2016), it is conceivable that lateral growth occurs at the site late prenatally and even during infancy. However, it was described as a degenerated mix of cartilage and fibrous tissue at birth by Bosma (1986), and thus there may be cause to doubt its role as a postnatal growth center in humans, pending more thorough histological study. The ABS (note: lower case abbreviation in figure legends) has received little histological assessment in non-human primates until recently. Smith et al. (2021a) found it remains cartilaginous at birth in some but not all primates; in some species it persists into infancy (e.g., *Otolemur crassicaudatus*, *Saguinus oedipus*), whereas in others it degenerates or ossifies before birth (*Varecia* spp.; *Eulemur* spp.) or perinatally (*Saimiri boliviensis*).

Goals of the present study

Our ability to generalize about sphenoid development in primates is limited since we have developmental stages of so few primate taxa. Measurements of the developing sphenoid bone in non-human primates are even more rare, focusing only on selected catarrhine species in the past (e.g., Moore 1978). Although early fetal stages of

chondrocranial development have been studied in numerous mammals (e.g., de Beer 1937; Sánchez-Villagra and Forasiepi 2017), some novel features of the sphenoid are not apparent at early stages. Moreover, dissimilar developmental characteristics are known to reflect character state reversals that occur during ontogeny within a species (e.g., foramen rotundum of *Tupaia* – Zeller, 1987). Resolving this confusion requires an understanding of development in a broader array of species. In addition, we require an understanding of a broad age range to fully understand how divergent development may be among taxa. In this regard, Presley (1993) discussed the hazards of preconceiving that the taxa we know best (e.g., *Homo*) are good models for understanding mammalian development in a broad sense. Thus, more ontogenetic study is needed, especially of non-human primates.

Our need for more comparative developmental information on the primate sphenoid relates to its key role as an interface among developing regions of the cranium. Because of the sphenoid bone’s location with the midline cranial skeleton, it has been hypothesized that the degree of midfacial projection hinges in large part on the orientation of basicranial interface with the midface (e.g., Scott 1958; Lieberman et al. 2000), or based on the primary direction of growth within the synchondrosis that unites the two regions (Smith et al. 2017). In addition, the bilateral elements of the sphenoid bone participate in joints with the calvaria that are of phylogenetic significance in primates (e.g., Fulwood et al. 2016) and have bilateral synchondroses with the basisphenoid, which remain unexplored in their development. Here, we reexamine the notion that basicranial development in *Homo* is unique compared to other primates, specifically regarding the pace of fusion of synchondroses (Lieberman et al. 2000). In addition, selected prenatal and newborn primates are studied for evidence of chondrocyte proliferation and hypertrophy at fetal and early postnatal ages, to establish when these joints exhibit growth potential, as evidenced by organized zones of proliferating and hypertrophic chondrocytes (see Smith et al., 2021a).

Table 2. Measurements (in mm) of the cranium and sphenoid in developing *Lemur catta* and *Saguinus* spp.

Specimen (age*)	CL*	ISSL	SL	PSL	BSL	PSW1	PSW2	BSW1	BSW2
<i>Lemur catta</i>									
fetal (2)	32.4	1.06	5.80	2.18	2.54	1.96	2.87	3.12	3.29
newborn (2)	40.6	0.97	7.29	2.71	3.75	1.97	2.39	2.75	3.24
infant (2)	47.8	0.767	9.62	4.23	4.71	1.92	2.97	3.15	3.57
<i>Saguinus geoffroyi</i>									
fetal (1)	21.3	1.51	3.67	0.97	1.42	0.81	0.75	1.24	1.51
newborn (1)	34.9	0.53	7.79	4.45	2.86	0.53	1.50	1.56	2.19
<i>Saguinus oedipus</i>									
Newborn (7)	31.7	0.53	6.73	3.76	2.41	0.72	1.47	1.45	1.74
infant (1)	33.6	0.31	8.29	4.88	3.15	0.78	1.77	1.73	1.96

*: here, “newborns” were up to 7 days postnatal (see Smith et al. 2020); “infants” in this study were between 19 and 30 days postnatal age; BSW1, basisphenoid length 1: width of anterior end; BSW2, basisphenoid length 2: width of posterior end. CL, cranial length (prosthion-inion); ISSL, anteroposterior length of intrasphenoidal synchondrosis; PSL, presphenoid length; BSL, basisphenoid length; PSW1, presphenoid length 1: width of anterior end; PSW2, presphenoid length 2: width of posterior end; SL; total sphenoid length; cranial length is based on larger samples of newborns as reported in Smith et al. 2020.

Materials and Methods

Sample

Individuals in the cadaveric sample used in this study were obtained after death by natural causes in captivity (Table 1). All specimens were fixed in formalin by immersion, or were frozen and then subsequently formalin-fixed. In sum, 39 cadavers were studied, some of which were previously sectioned (e.g., Smith et al. 2015, 2021a), and some newly prepared for the present study. In addition, one sectioned prenatal loris (*Nycticebus coucang*), estimated to be at an early fetal stage of development, was available for study from the Hubrecht collection (Table 1). The prenatal specimens examined are not stage-matched among the species, a difficult aim even with more common primates. The youngest prenatal primate in our sample, *Nycticebus*, has a fully fused palate, but little ossification of the chondrocranium, and the body (based on museum photographs) remains highly flexed. This specimen is judged to be early fetal. The fetal *Loris* specimens are considerably more advanced in basicranial ossification and may be midgestation. Prenatal *Lemur* and *Saguinus* were assessed to be fetal based on relative head size compared to known newborns (Table 2). Furthermore, the *Lemur* specimen was recorded stillborn at “12–18 days preterm” at Duke Lemur Center, Durham, NC, U.S.A. Throughout the text, “newborns” or “neonates” are specimens of known age or similar to specimens of known age up to 7 days postnatal (see Smith et al. 2020 for further discussion on aging). “Infants” are also of known age, and in this sample all are between 19 and 30 days postnatal age (Table 1; Suppl. Tables S1, S2).

Most specimens were scanned using microcomputed tomography (μ CT). Scanning was conducted at Northeast Ohio Medical University (NEOMED) using a Scanco vivaCT 75 scanner (scan parameters: 70 kVp; 114 mA; 380 ms exposure time). The volumes were reconstruct-

ed using 20.5–30 μ m cubic voxels (depending on head size) and exported as 2048×2048 8-bit TIFF stacks for three-dimensional reconstructions (DeLeon and Smith 2014). All three-dimensional reconstructions were carried out using Amira 2019.1 software (Thermo Fisher Scientific). Segmentations were carried out automatically via the magic wand tool, to establish basicranial contours for measurements, and then separately to isolate the sphenoid bone. PLY files of selected specimens can be viewed at the following <https://www.morphosource.org/projects/000367594?locale=en>.

Histological and immunohistochemical methods

A subset of the sample was serially sectioned, including an age range (based on known ages or surmised based on varying head sizes) for *Saguinus* spp. (9 specimens), *Saimiri boliviensis* (8), *Loris tardigradus* (1), *Otolemur crassicaudatus* (2) and *Varecia* spp. (4). In most cases, one half of the head was sectioned in a sagittal plane in order to examine the midline synchondroses. The contralateral side was sectioned in either a coronal or horizontal plane, which enabled a better understanding of the orientation of the ABS. Routine paraffin embedding followed decalcification in a formic acid-sodium citrate solution. Sections were at 10 μ m thickness, and every fourth to tenth section was mounted on glass slides. Slides were alternately stained using Gomori trichrome or hematoxylin-eosin procedures (for more details see DeLeon and Smith 2014). Serial sections were examined by light microscopy using a Zeiss stereo microscope (X0.64 to X1.6 magnification) or a Leica DMLB photomicroscope (X25 to X630). Selected sections were photographed using an Axiocam MRc 5 Firewire camera attached to the Leica microscope) or a MRc 150 Firewire camera (attached to the Zeiss microscope).

Fetal and newborn specimens of *Saguinus* spp. (5), fetal *Lemur catta* (1), and newborn *Varecia variegata*

(1) were immunohistochemically studied to establish the mitotic characteristics of chondrocytes within sphenoidal synchondroses. The specimens were prepared using immunohistochemistry to detect proliferating cell nuclear antigen (PCNA), a marker of mitotic cells. Briefly, sections were deparaffinized and rehydrated to water. A short antigen retrieval step was accomplished in boiling Sodium Citrate Buffer for 2 minutes followed by cooling. Endogenous peroxidase was blocked with 3% hydrogen peroxide in methanol, and then 1% Goat Serum was used to block non-specific binding. Sections were then incubated with PCNA primary antibody (AbCam, Cambridge, MA, USA, ab18197) diluted 1 to 3000 in Goat Serum for 2 hours at room temperature. After three washes with Phosphate-Buffered Saline (PBS) sections were incubated with Goat Anti-Rabbit Secondary Antibody conjugated for HRP (AbCam, ab6721) for 1 hour at room temperature and were subsequently washed again with PBS three times. Finally, sections were exposed to 3,3'-diaminobenzidine (DAB) (Vector Laboratories, Bullingame, CA, USA) for 3 minutes, the reaction was stopped with water. Most sections were also counterstained with Fast Green 0.1% solution diluted 1:10 in water and the sections were dehydrated, cleared, and mounted with permount (Fisher Scientific, Waltham, MA, USA). Selected sections of each specimen were also prepared as negative controls, in which the primary antibody was omitted. In most negative controls, DAB staining was barely detected; only one control slide revealed reactivity to nuclei, but the reactivity was still far less than in the slides for which the primary antibody was present (Suppl. Fig. S1).

Histological and μ CT alignment and investigation

In selected cases, μ CT scan volumes were manually rotated until the slice planes were aligned to histology sections of the same specimen. This was accomplished using Amira software. Approximate matches were sought, focusing on the sphenoid bone and in particular the contours of developing foramina. Subsequently, every 4th to 5th histology section was matched to corresponding μ CT slices. Matching histology and μ CT sections/slices were then opened in Photoshop, and the histology was resized and pasted onto the CT slice, made partially transparent, manually rotated into alignment with the μ CT slice, and then made opaque and saved as a new file name. This was done for all μ CT slices containing the sphenoid bone, and some space anteriorly and posteriorly. Then, using Amira, segmentation of the sphenoid bone was accomplished, using the μ CT slices overlaid with aligned histology (see below).

Trigeminal nerve branches were traced to infer the extent to which foramina are formed by the cartilaginous template of the sphenoid as opposed to expansion of appositional bone. Across vertebrates, the relationship of the basicranium to the branches of the trigeminal nerve and associated ganglia have drawn attention for decades (e.g., de Beer 1929; Maier 1987; Presley 1993; Yamamoto et al. 2018). A major distinction between reptiles and

mammals is the location of the initial roots of primary trigeminal branches and the trigeminal ganglia, which are housed completely within the skull of mammals, owing to a secondarily formed neurocranial wall. In reptiles, by contrast these neural elements are outside of the neurocranium (Maier 1987). The specific relationship of trigeminal branches to parts of the sphenoid anlagen have been revealed to vary, even within mammals (Maier 1987). Thus, while the trigeminal nerve branches exit in identically named foramina in many mammals, it may not develop in precisely the same way. Foramina may or may not be surrounded by cartilage during development (membranous bone completes the boundary of some foramina). Further complicating the nerve-to bone topography is that whereas a nerve branch may initially be encircled by cartilage of a chondrocranial element, portions of cartilage may regress during development, and be replaced by de novo membranous bone (e.g., Zeller 1987). In addition, the nerve to the pterygoid canal (Vidian nerve) was traced based on its position close to the interface of the basi- and alisphenoid elements. This nerve passes close to the basitrabecular process of the basisphenoid (de Beer 1929), to which the ABS is connected (Maier 1993; Smith et al. 2021a). Thus, the Vidian nerve serves as a useful landmark to identify the alibasisphenoidal synchondrosis before or after it fuses.

μ CT-based metric comparisons

Cranial measurements were made on two primate genera (*Saguinus geoffroyi*, *S. oedipus* and *Lemur catta*) for which we had prenatal and early postnatal stages (Table 2; Suppl. Table S1). The sample sizes are small and thus interpreted with caution. To bolster samples of *Lemur catta*, we used one specimen of unrecorded age, which matched the size and dental eruption status of a fetal specimen that was of known gestational age. Some previously sectioned specimens had been measured using calipers to obtain cranial (prosthion-inion) and palatal (prosthion-posterior midpalatal point) length (Smith et al. 2015). For most specimens these measurements were acquired digitally using Amira, after segmentation and reconstruction. In addition, sphenoid, basisphenoid, presphenoid, and ISS lengths were measured on the ectocranial sides of the bones. Width of the presphenoid and basisphenoid were measured at the anterior and posterior ends. These measurements were used to track differences in proportions at fetal, newborn and infant ages (Tables 3–4).

Results

Comparative histogenesis of the primate sphenoid bone during early to midfetal ontogeny

The early fetal slow loris (*Nycticebus coucang*) has little ossification of the chondrocranium, which still possesses the cartilaginous precursors for the sphenoid bodies and for the alisphenoid (Fig. 1A). The cartilage is dense with chondrocytes, virtually devoid of extracellular matrix. Small patches of perichondrial bone can be seen bordering parts of the ala temporalis (Fig. 1B). Posteriorly the ala temporalis becomes smaller (Fig. 1C) and is connected to the alar process of the lamina hypophyseos (Fig. 1D). The Vidian nerve passes in proximity to the alar process and the medial margin of the ala temporalis. Posteriorly, near its origin at the intersection of the deep and greater petrosal nerves, it passes inferior to these structures (Figs 1C, D). Anteriorly, at the level of the lamina trabecularis (site of future presphenoid body) the nerve penetrates the ala temporalis from beneath, and courses posteriorly before exiting on the superior side (Fig. 1A).

In a later stage, fetal slender loris (*Loris tardigradus*), the sphenoid has three separate ossified components, the basisphenoid body, the alisphenoid-ptyergoid complex, and the fused presphenoid-orbitosphenoid (Fig. 2). The alisphenoid is extensively ossified but has persisting cartilage at the base of the lateral and medial pterygoid plates (Fig. 2A). The basisphenoid and alisphenoid are united by an elongated ABS, which is the remnant of the alar process of the hypophyseal plate, as indicated by the persisting relationship with the Vidian nerve (Fig. 2B). By tracing the lateral edge of the ABS (Fig. 2C), one can also observe bone of perichondrial origin that spreads laterally as the membranous part of the alisphenoid.

Comparative morphogenesis of the sphenoid bone from late fetal and newborn stages

The ABS is widely patent in the fetal *Lemur catta*, connecting the basitrabecular process of the basisphenoid with the alisphenoid (Fig. 3A–B); its breadth is easier to appreciate in histological sections (Fig. 3C) than in μ CT reconstructions. The axis of chondrocyte columns in the ABS of the fetus lies within the coronal plane. It has a bipolar organization with proliferating chondrocytes (Fig. 3C), most of which are PCNA positive (not shown). In the fetus, histological sections indicate that no cartilage remains in the orbitosphenoid.

Compared to the late fetal *Lemur catta*, in the newborn both the ISS and ABS become reduced; no trace of cartilage can be found at the ABS in one serially sectioned newborn (histology not shown). At birth, the alisphenoid bone is greatly expanded anteroposteriorly (Fig. 3D). The alisphenoid, basisphenoid, and presphenoid all become proportionally more elongated anteroposteriorly in the

newborn. The orbitosphenoid enlarges less by comparison. Organization of midline synchondroses in *Varecia* spp. was previously described (Smith et al. 2021a); here we confirm PCNA-reactivity in the proliferating chondrocytes zone of all midline synchondroses at birth. A newborn *Varecia* exhibited PCNA-reactive chondrocytes within SOS (Suppl. Fig. S2A). The chondrocytes were lightly-labeled, perhaps due to lengthy fixation in formalin over decades. However, the chondrocytes were above the background level in control slides (Suppl. Fig. S2B).

In *Saguinus geoffroyi*, there is remarkable reduction of intrasphenoid synchondrosis and ABS from fetal to newborn stages of development. Because the *Saguinus* fetus is not a late stage, the magnitude of reduction is much greater than observed in fetal vs. newborn *Lemur catta*. Ratios of ISS length to total anteroposterior sphenoid length reveal a large difference in the ISS between ages. In the fetus, the ISS comprises 41% of the midline length of the sphenoid (Table 3), whereas in the newborn the ISS is reduced to ~7% of sphenoid length. The proportions of the pre- and basisphenoid bodies also differ greatly, with the width/length ratio of each being far smaller in the newborn, especially for the presphenoid (Table 4). This reflects a great elongation of each bone proportionally. The ABS is oriented anterolaterally, and across age, the growth of the alisphenoid bone expands in all directions, but notably in anteroposterior breadth (Fig. 4).

In the fetal *Saguinus geoffroyi*, the presphenoid, basisphenoid, alisphenoid, and orbitosphenoid are separate elements (Figs 4C, 5A), the latter represented only by a metoptic root. By comparison to the newborn (Fig. 4D), the alisphenoid is anteroposteriorly reduced in the fetus. The basitrabecular process is a prominent spike, directed laterally (Fig. 4C) as observed in the late fetus as well as in the newborn specimen. Both the intrasphenoid and ABS are greatly reduced in the newborn (Figs 4B, D).

Based on a comparison of earlier to later stages, the sphenoid bone of *Saguinus* spp. is proportionally longer in the older specimens with a relatively reduced ISS (Table 2). The ISS is narrower in the newborn (Fig. 5B, D) compared to the fetus (Fig. 5A, C). Histology indicates it remains an active growth center at birth. There are a greater number of cells and absolute length in the proliferating and hypertrophic zones in the fetus (Fig. 5E) as opposed to the newborn (Fig. 5F). In both the ISS and PSept, the proliferating zone is shorter by more than 50% in absolute length in newborns (Figs 5F, H) compared to the fetus (Figs 5E, G). In the fetus, PCNA is expressed by cells throughout the proliferating zone and by chondrocytes in numerous rows of the hypertrophic zone (Figs 5E, G). In the newborn, proliferating chondrocytes and only a restricted number of hypertrophic chondrocytes, nearest to the proliferating zone, are PCNA positive (Figs 5F, H).

The ABS was PCNA-reactive at birth as well, but the organization of proliferating chondrocytes was more difficult to visualize in newborns (Fig. 6E, inset) than in the fetus (Fig. 6C). Older infant specimens were not studied here using immunohistochemistry, pending a broader cross-sectional age study.

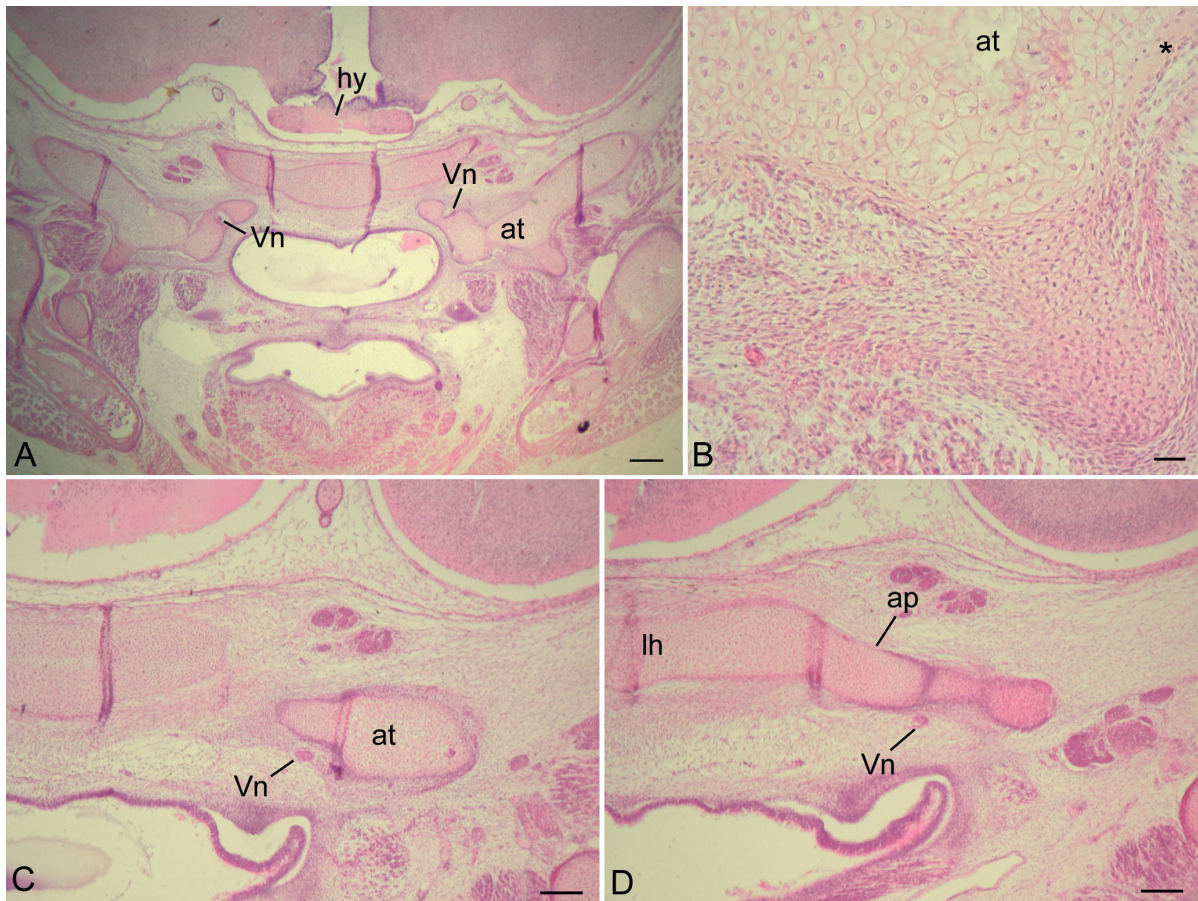


Figure 1. Histology of prenatal *Nycticebus coucang* sphenoid bone, as seen in coronal sections. A) Anterior aspect of developing sphenoid region, where the Vidian nerve (vn) passes medially and superiorly to ala temporalis (at). B) Magnified view of AT, same section as plate a, revealing densely-packed chondrocytes, and newly formed perichondrial bone (*). C) A more posterior section shows the alate temporalis to be much smaller, and further posteriorly (D) it connects to the alar process (ap) of the lamina hypophyseos (lh); here, the Vidian nerve passes inferiorly. Further abbreviations: hy, hypophysis. Scale bars: A, 250 μ m; B, 30 μ m; C, D, 150 μ m.

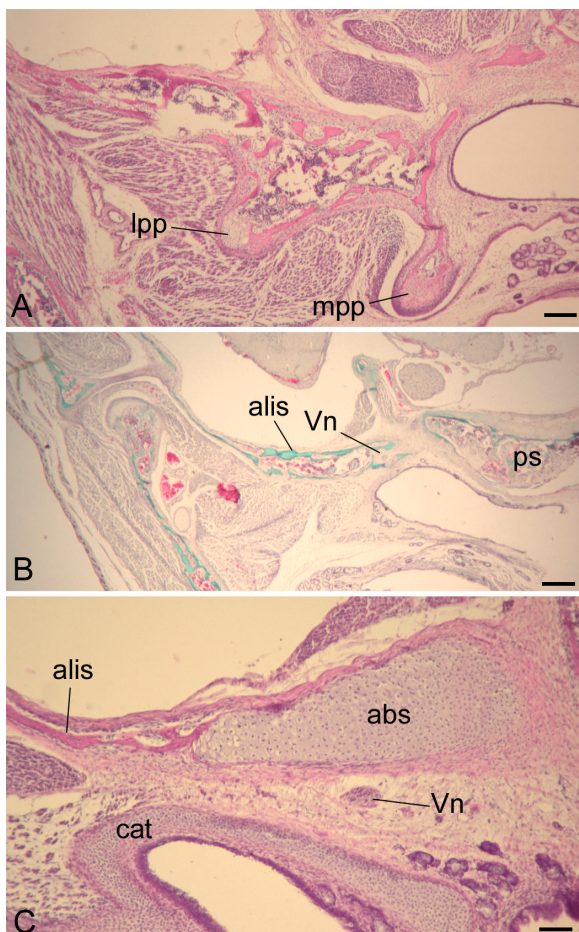


Figure 2. Histology of three components of sphenoid bone in fetal *Loris tardigradus*, as seen in the coronal plane. A) Cartilage shown at bases of medial pterygoid (mpp), lateral pterygoid plates (lpp), and the alisphenoid (alis). B) The alisphenoid projects anterior to the basisphenoids, adjacent to the presphenoid (ps). Here the Vidian nerve (Vn) can be seen near its departure from the pterygoid canal. C) The alibasisphenoidal synchondrosis (abs), with membranous expansion of the alisphenoid emanating from its lateral limit. The Vidian nerve is inferior to the abs. Further abbreviations: cat, cartilage of the auditory tube. Stains: a, c, hematoxylin and eosin; b, Gomori trichrome. Scale bars: A, 150 μ m; B, 300 μ m; C, 75 μ m.

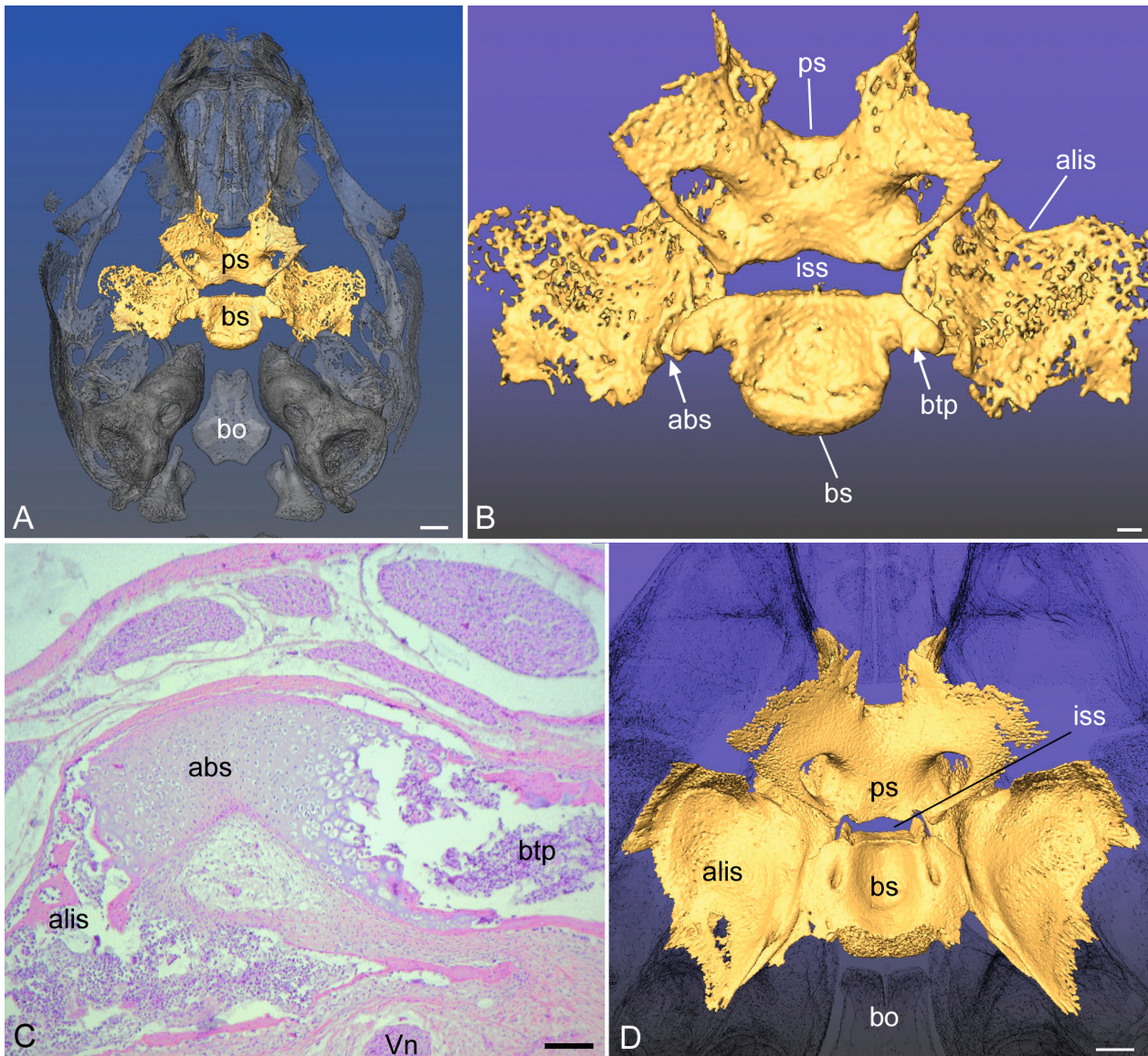


Figure 3. Fetal (A, B, C) compared to newborn (D) *Lemur catta*. A) The sphenoid bones are in the dorsal view, with ghosted skull for context. B) A more magnified view of the fetus reveals the basitrabecular process (btp) of the basisphenoids, positioned adjacent to the alibasisphenoidal synchondrosis (abs). The gap at the abs is difficult to discern osteologically, but histology (C) reveals it clearly, bridging the basisphenoid (bs) and alisphenoid. Note the Vidian nerve (Vn) approaching the posterior side of the pterygoid canal from below. D) In the newborn, histology (not shown) reveals no vestige of the cartilage of the abs. The basitrabecular process is still apparent. Note that the intrasphenoidal synchondrosis (iss) is proportionally reduced in the newborn compared to the fetus. Further abbreviations: bo, basioccipital; ps, presphenoid. Scale bars: A, 1.5 mm; B, 0.5 mm; C, 200 μ m; D, 1.5 mm.

When histologically sectioned in the coronal plane, the ABS of fetal *Saguinus geoffroyi* appears as a roughly oval cartilaginous mass (Suppl. Fig. S3), in which organization of the chondrocytes is not discernable. Sagittal sections reveal the ABS in a longitudinal view (Suppl. Fig. S3; Figs 6A, B). Chondrocytes are clearly organized into proliferating and hypertrophic columns; proliferating chondrocytes and the first rows of hypertrophic chondrocytes are PCNA-reactive (Fig. 6C). At birth, the ABS of *Saguinus geoffroyi* or *Saguinus oedipus* has fewer rows of proliferating chondrocytes than in the fetus. It is also redirected to be oblique, oriented anteroinferiorly, within the sagittal plane (Fig. 6D). The organization is bipolar. However, proliferating chondrocytes are no longer well-organized into columns, and fewer hypertrophic

chondrocytes are visible (Fig. 6E). PCNA reactivity is still visible (Fig. 6E, inset), but not consistently near the ossification front.

Early postnatal morphogenesis of the sphenoid

Perinatally, the ISS is widely patent in all strepsirrhines examined here (Fig. 8). In *Lemur*, the ISS comprises nearly 20% of the anteroposterior length of the sphenoid bone in the smallest (late fetal) specimens (see Table 3). This percentage decreases in newborns (~13%) and still more in infants (~8%) (Table 3). A stark difference exists in absolute dimensions of the sphenoid bone in fetal compared

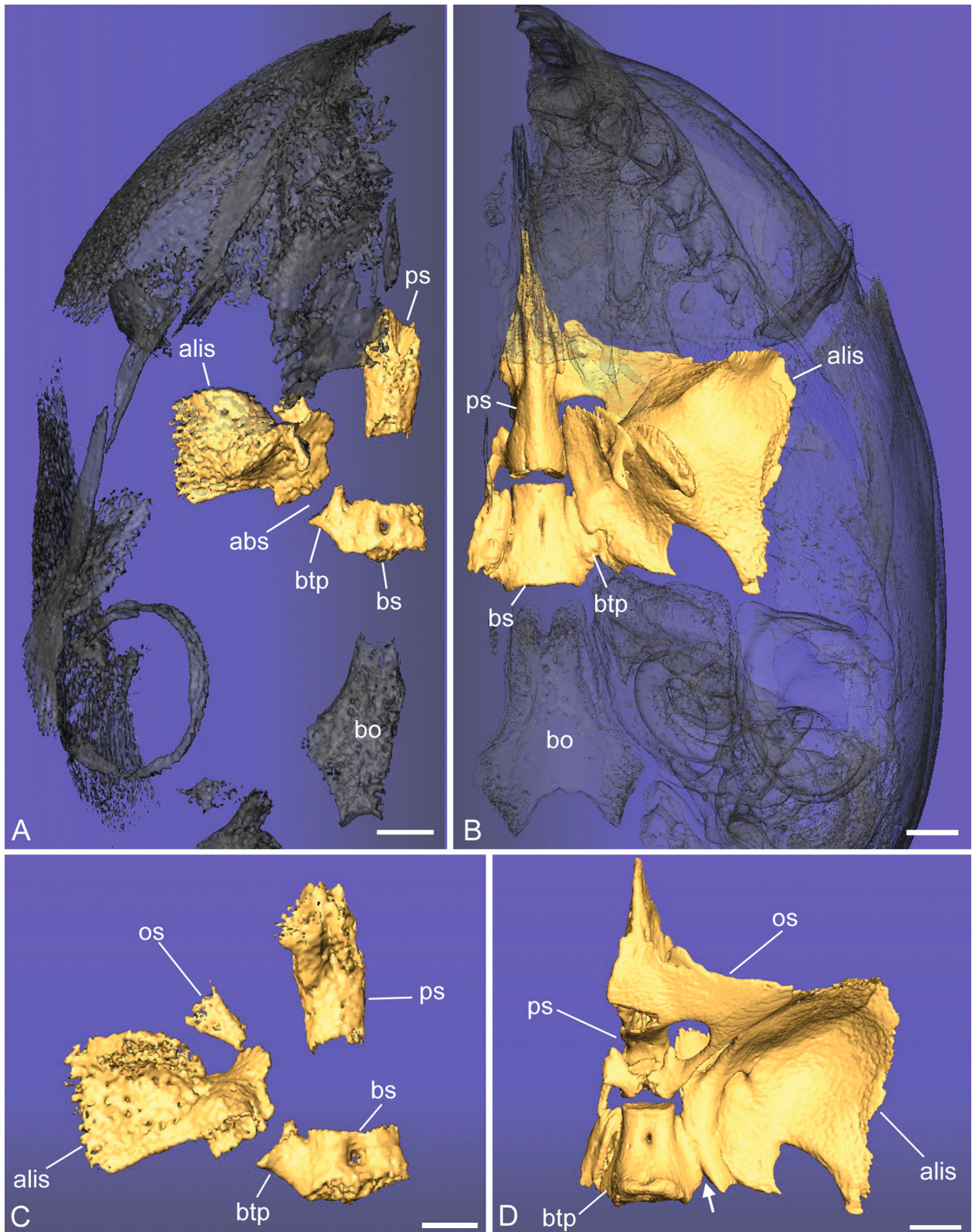


Figure 4. Fetal (A, C) and newborn (B, D) specimens of *Saguinus geoffroyi*. A, B) The sphenoid bone is shown in ventral view, with the whole skull in ghosted view. Note the marked decreased distance between the basisphenoid (bs) and presphenoid (ps). Also note that the alibasisphenoidal synchondrosis (abs), between the basisphenoid and the alisphenoid (alis), oriented laterally but also anteriorly in the fetus, appears fused or nearly so at birth. C, D) Enlarged dorsal views show the degree of ossification of the sphenoid overall. The fetal specimen has a more precociously ossified basisphenoid and alisphenoid relative to the presphenoid and orbitosphenoid (os). In the enlarged view of the fetus (C), the orbitosphenoid is shown to be in a very early point in ossification; the ossified element is the inferior (metoptic) root. Also note the position of the basitrabecular process (btp), located at the posterior margin of the abs. This landmark can also be seen in the newborn (D, arrows), but the synchondrosis is greatly reduced at birth. Further abbreviations: bo, basioccipital. Scale bars: A, 1 mm; B, 1.5 mm; C, 750 μ m; D, 1.5 mm.

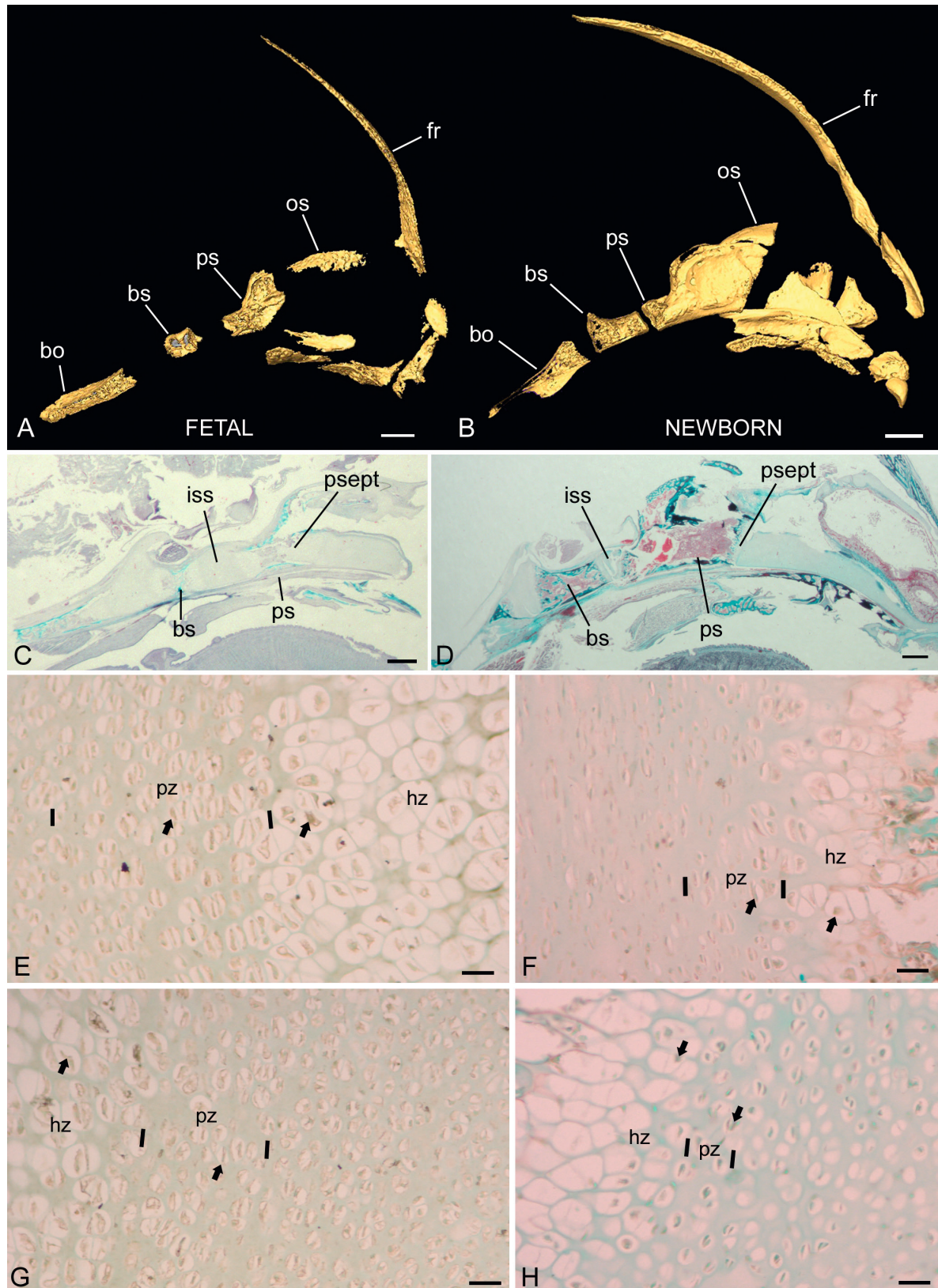


Figure 5. Fetal (left side) and newborn (right side) midline synchondroses in *Saguinus* spp. A, B) Midline segments of *Saguinus Geoffroyi* crania are shown at the two ages revealing the decreased space between the presphenoid (ps) and basisphenoid (bs) bones in the newborn (B) compared to the fetus (A). C, D) low magnification views of the midline synchondroses in the fetus (C, same specimen as A) and a newborn (D, *S. oedipus* used instead due to better preservation); both stained with Gomori trichrome procedure. Indicated are the intrasphenoidal (iss) and presphenoseptal (psept) synchondroses. Below, higher magnifications of the iss (E, F) and psept (G, H) at the same ages, prepared using PCNA immunohistochemistry, with fast green counterstain. Since all higher magnification images are at the same magnification, it is clear that the absolute length of the zones of proliferating (pz) and hypertrophic (hz) chondrocytes is reduced in the newborn compared to the fetus. Further abbreviations: fr, frontal; os, orbitosphenoid; bo, basioccipital. Scale bars: A, 1 mm; B, 2 mm; C, D, 1 mm; E–H, 30 μ m.

Table 3. Differences in cranial and sphenoid dimensions between specimens of fetal, newborn and one-month-old *Lemur catta* and *Saguinus* spp.

	% difference between age groups				
	CL	ISSL	SL	PSL	BSL
<i>Lemur catta</i>					
fetal to newborn	24.24	-8.53	25.81	24.31	47.06
newborn to infant	18.64	-20.86	31.76	56.27	25.68
<i>Saguinus geoffroyi</i>					
fetal to newborn	64.05	-65.08	112.21	361.18	101.01
<i>Saguinus oedipus</i>					
newborn to infant	6.10	-38.51	21.40	34.50	3.74

BSL, basisphenoids length; CL, cranial length; ISSL, anteroposterior length of intrasphenoidal synchondrosis; PSL, presphenoid length; SL, total sphenoid length

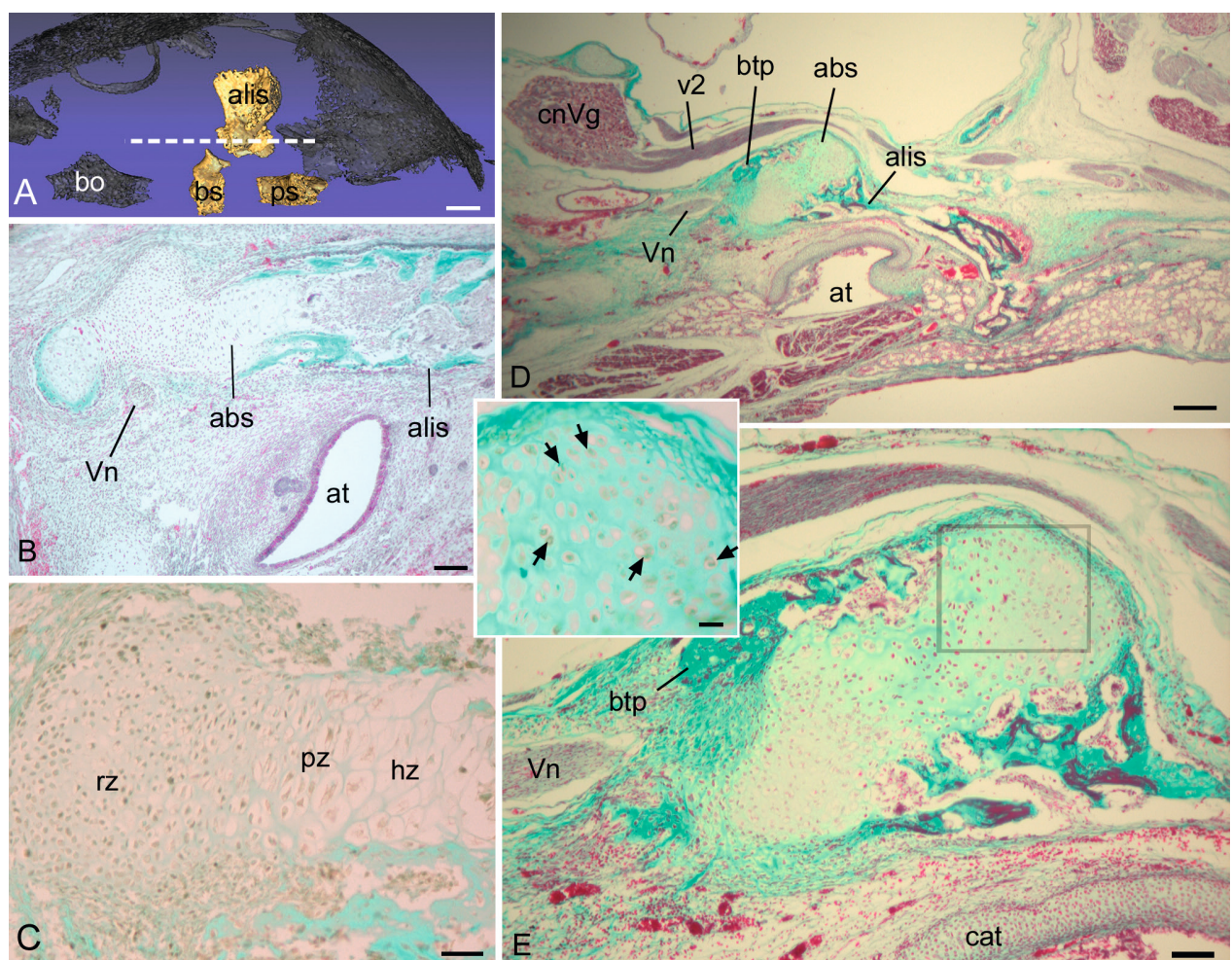


Figure 6. The alibasisphenoidal synchondrosis (abs) in late fetal *Saguinus geoffroyi* (A–C) and newborn *Saguinus oedipus* (D, E). A) The approximate level of the sagittal histological section of the fetal sphenoid bone is shown as a dashed line over the basal view of the skull (sphenoid emphasized, remainder of skull ghosted in black). B) A parasagittal section revealing an elongated abs. C) A section near the one shown in B shown at higher magnification, prepared using immunohistochemistry to PCNA, counterstained with fast green. Note chondrocytes in the reserve (rz) and proliferating zones (pz) are PCNA+, but most chondrocytes in the hypertrophic zone (hz) are PCNA-negative. D, E) low and higher magnifications of abs in newborn *S. oedipus*. Note the growth is now re-directed slightly inferiorly from the basitrabecular process (btp) of the basisphenoid bone, and the abs is proportionately shorter in anteroposterior breadth. Inset: A preparation of a nearby section to that in e (see box for specific location), made using immunohistochemistry to PCNA, counterstained with fast green. Multiple chondrocytes are PCNA+ (arrows), but few chondrocytes are organized into columns. Note the close relationship of abs to the Vidian nerve (Vn). Further abbreviations: alis, alisphenoid; at, auditory tube; bo, basioccipital; bs, basisphenoid; cat, auditory tube cartilage; cnVg, trigeminal ganglion; ps, presphenoid. Stains: Gomori trichrome, except for inset (see above). Scale bars: A, 1mm; B, 100 μ m; C, 40; D, 250 μ m; E, 80 μ m; inset, 20 μ m.

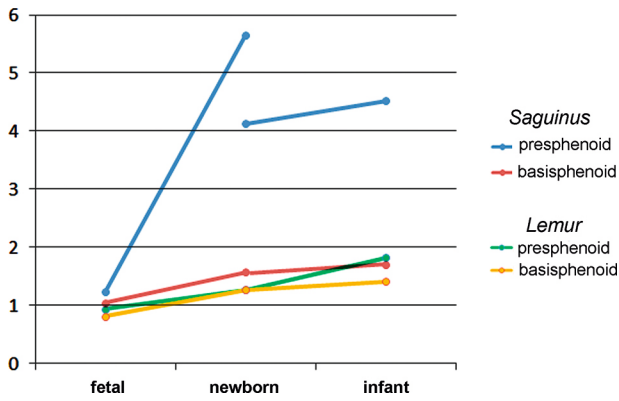


Figure 7. Length-width ratios of the presphenoid and basisphenoids shown across ages in subadult lemurs (*Lemur catta*) and tamarins (*Saguinus* spp.). The fetal to newborn data are from *Saguinus geoffroyi*, whereas the newborn to infant data are from *Saguinus oedipus*. Because the data are from two different species; there is some discrepancy between newborn data points for the presphenoid (by chance, this is not the case for the basisphenoid). The presphenoid stands out as a segment that is elongated (higher length-width ratio) compared to the basisphenoid; these preliminary data indicate this may be a proportional change during later fetal development

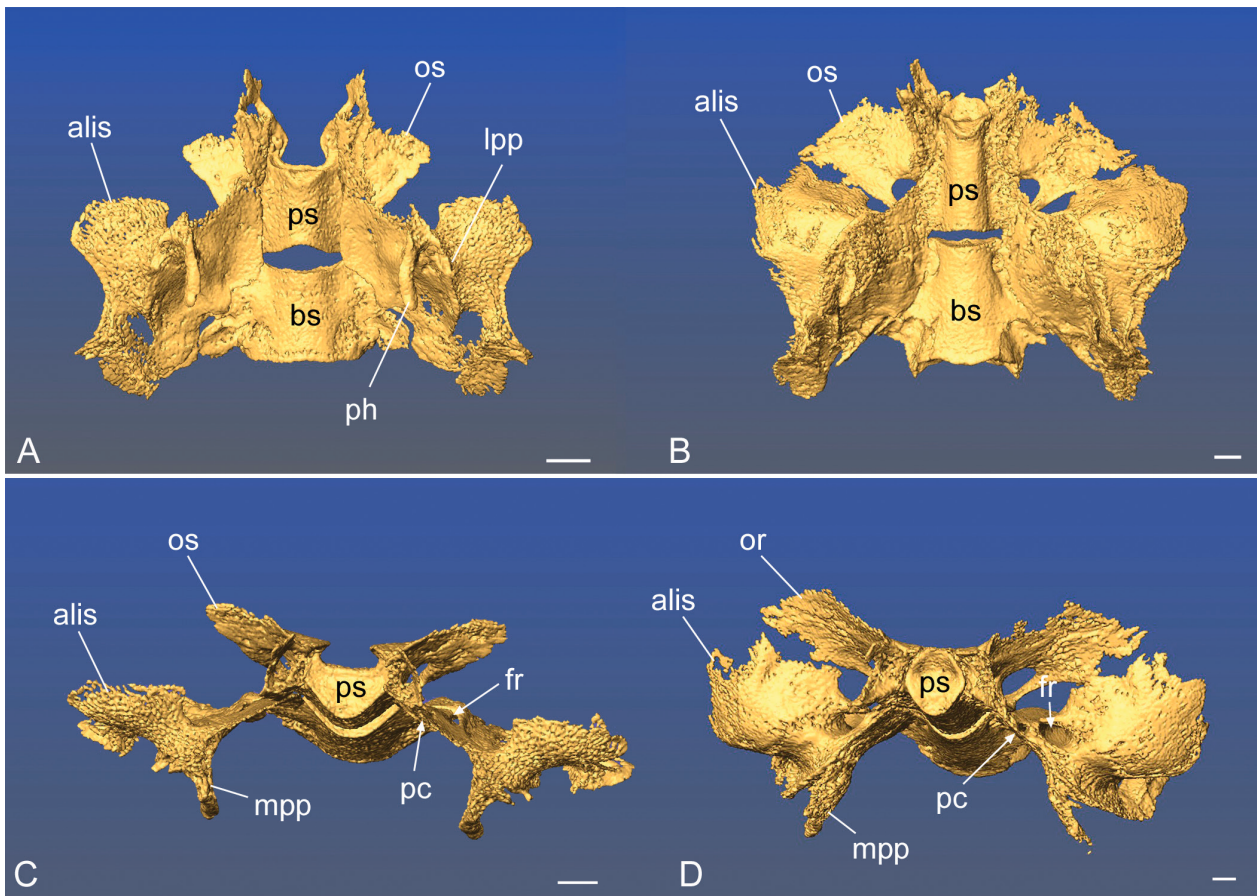


Figure 8. The sphenoid bone in two specimens of *Varecia* spp., revealing perinatal transformation of the different components of the bone. A, C) a stillborn specimen of *V. rubra* that was undersized compared to newborn specimens, and presumably at a late fetal stage. B, D), a 24-day-old infant *V. variegata*. The top row shows a ventral view, the bottom row shows an anterior view, slightly lateral to the left side. Further abbreviations: alis, alisphenoid; bs, basisphenoid; fr, foramen rotundum; mpp, medial pterygoid plate; lpp, lateral pterygoid plate; os, orbitosphenoid; ph, pterygoid hamulus; pc, pterygoid canal; ps, presphenoid. Scale bars: A, C, 1.5 mm; B, D, 1 mm.

to newborn *Saguinus geoffroyi*, and this reflects changing proportions of the bone. The length/width ratios of pre- and basisphenoids are near 1.2 in the fetus, but the relative length of the presphenoid drastically increases in the newborn (Table 4). In length, the increase in presphenoid length (361%) far exceeds that of other cranial measurements, including basisphenoid and overall cranial length (Table 3).

It should be noted that the comparison of fetal to newborn sphenoid dimensions are not analogous in the *Saguinus* spp. and *Lemur catta*. The prenatal *Saguinus geoffroyi* specimen is clearly a much earlier stage fetus than the prenatal *Lemur catta*; this is reflected in the % increase in cranial length (Table 3). However, unlike *Lemur catta*, in *Saguinus* spp. the % changes in presphenoid length scale much differently than % changes for basisphenoid length

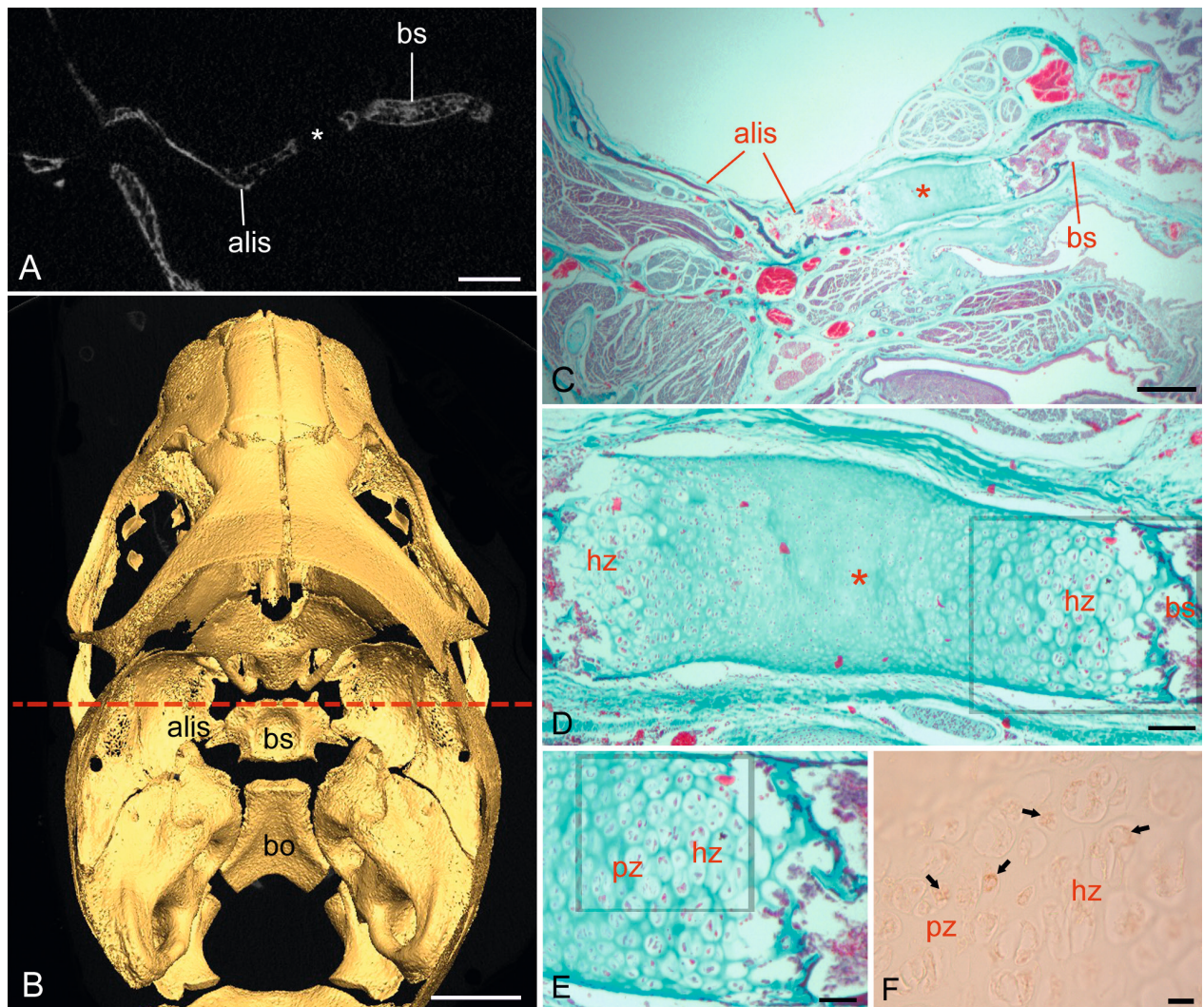


Figure 9. Late fetal cranium of *Otolemur crassicaudatus*, showing the synchondrosis (*) between the alisphenoid (alis) and basisphenoid (bs). The slice plane in CT at top left (A) is indicated by a red dashed line through the endocranial view of the skull (B). C) Histology from a twin sibling, closely matching the CT slice plane. D) A magnified view shows this is a bipolar synchondrosis, with a zone of hypertrophic chondrocytes (hz) adjacent to the alisphenoid and basisphenoid. E) A higher magnification view, enlarged from boxed area in D reveals rows of proliferating chondrocytes (pz) adjacent the hypertrophic zone. F) A higher magnification view in a nearby section is prepared with PCNA immunohistochemistry. Note PCNA-reactive chondrocytes (arrows), which are strongly reactive in proliferating chondrocytes and moderately in hypertrophic chondrocytes (box in (E) shows the approximate location of plate f). Further abbreviations: bo, basioccipital. Scale bars: A, 1.5 mm; B, 4 mm; C, 0.5 mm; D, 100 μ m; E, 50 μ m; f, 10 μ m.

(Fig. 7). This implies growth of the sphenoid segments is more closely isometric in *Lemur*.

The sphenoid bone of the newborn *Varecia rubra* is relatively narrower in width and anteroposteriorly longer than the late fetal *Varecia rubra*, and especially so compared to the older infant *Varecia variegata* (Fig. 8). This same contrast applies to the presphenoid and basisphenoid bodies as well. This is quantifiable in the cross-sectional age series of *Lemur*. The width/length ratio of the pre- and basisphenoid bodies decreases progressively in newborn compared to fetal specimens, and to a lesser extent in infant compared to newborn specimens (Table 2). Across age, the orbitosphenoids increase greatly in breadth, whereas the alisphenoids expand superiorly at the anterior and anterolateral sides (Fig. 8).

Neither of the lemurids has a widely patent ABS at birth. In contrast, the ABS is widely patent in late fetal

Otolemur (Fig. 9). This specimen, at ~ 90 % of average head length for newborn *Otolemur crassicaudatus*, has well-organized columns of proliferating and hypertrophic chondrocytes, with some chondrocytes expressing reactivity to PCNA antibodies (Figs 9E, F). A newborn *Otolemur crassicaudatus* also possesses a wide ABS. In both specimens, which are close in cranial length (Table 1), the average (right and left) transverse breadth of the ABS is just less than 1 mm. In an infant (not histologically sectioned), the gap at ABS has narrowed considerably, measuring an average of 0.2 mm in transverse breadth (Suppl. Fig. S4).

The proportions of the bodies appear to differ little between newborns and the older infant *Saguinus oedipus*, and this is supported by the slight difference in width to length ratios of the pre- and basisphenoid (Table 4). The ISS decreases slightly, as a percentage of total sphenoid

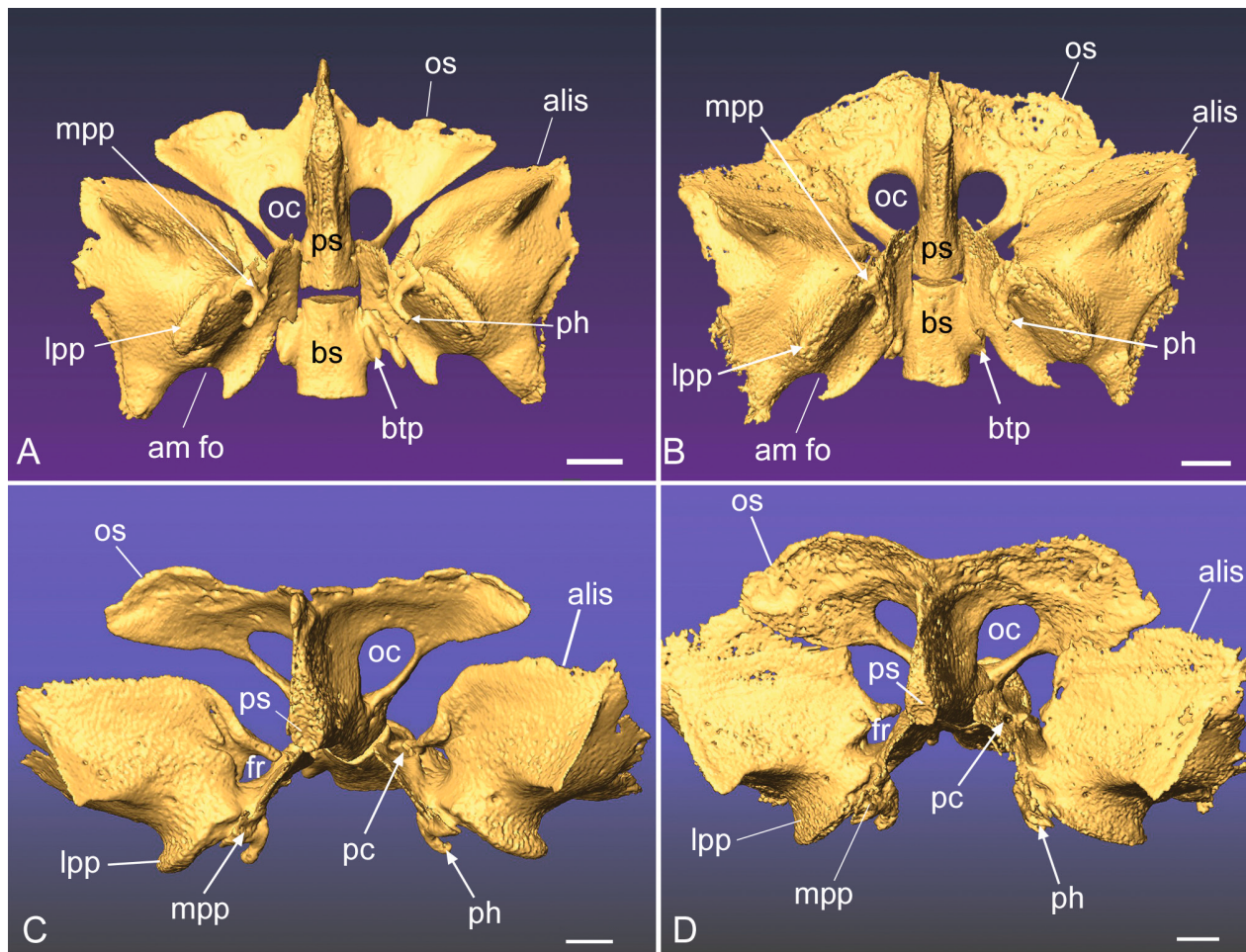


Figure 10. Transformation of *Saguinus oedipus* sphenoid bone comparing newborn (A, C) and one-month-old (B, D) displaying different components of bone. Images presented in ventral (top row) and slight anterolateral view (bottom row). Further abbreviations: alis, alisphenoid; amfo, anterior margin foramen ovale; bs, basisphenoid; mpp, medial pterygoid plate; lpp, lateral pterygoid plate; ph, pterygoid hamulus; ps, presphenoid; oc, optic canal; os, orbitosphenoid; pc, pterygoid canal; fr, foramen rotundum. Scale bars, 1.5 mm.

length (Table 3). Across age, the orbitosphenoid increases in breadth and the anterolateral sides of the alisphenoid expand superiorly. Ossification is more progressed overall at one-month, including anterior and lateral expansion of the alisphenoid and orbitosphenoid. Additionally, the pterygoid canal of the newborn is not fully enclosed, but is more fully enclosed at one-month (Fig. 10). Correspondingly, cartilage within the ABS synchondrosis is markedly reduced at one-month of age, appearing to consist only of small islands of cartilage at the joint site.

The sample of *Saimiri boliviensis* is a narrower age range, and midline synchondroses are similar to those of *Saguinus* (e.g., bipolar ISS), which were previously described (Smith et al., 2021a). However, the ABS is variable in our sample. Cartilage remains in the ABS in 5 of 8 specimens that were serially sectioned. The specimen with the smallest head size also has the widest separation between the alisphenoid and basisphenoid (Figs 11A–C). As in perinatal *Saguinus*, the cartilaginous ABS has a slightly downward and lateral trajectory. Yet, when histology is superimposed over CT slices and three-dimensionally reconstructed (Figs 11D–E), the ABS is shown to primarily orient anteroposteriorly, as in newborn *Saguinus* spp. The

spatial relationships to branches of the trigeminal and Vidian nerves (Figs 11C, 11F) and auditory tube (Fig. 11C) are precisely the same as in *Saguinus* (Fig. 6D).

Discussion

Our knowledge of comparative developmental anatomy of the sphenoid bone is mostly heavily centered on late embryonic and early fetal stages (e.g., see de Beer 1937; Starck 1975; Schunke and Zeller 2010; Sánchez-Villagra and Forasiepi 2017). In the developing skull, the chondrocranium comprises the cartilaginous portion of the cranial endoskeleton, and includes the template for basicranial bones as well as capsules for the special senses of hearing, balance and smell (Kawasaki and Richtsmeier 2017; Pitirri et al. 2020; Smith et al. 2020; Werneburg 2020). It spans rostrocaudal space from the endochondral part of the occipital bone to the external nasal cartilages of the nose (Maier 1993, 2000; Maier 2020a; Pitirri et al. 2020; Ruf 2020).

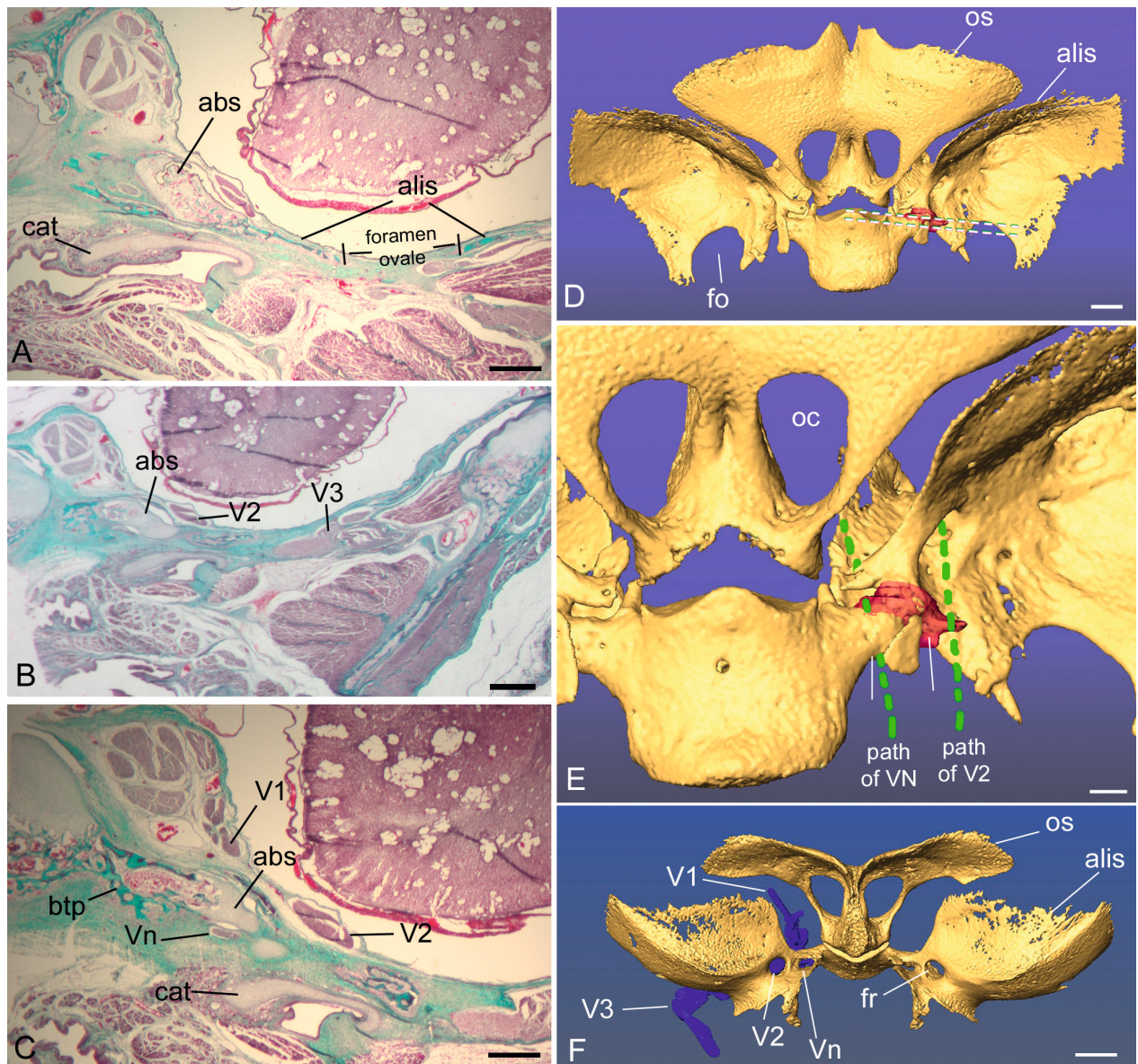


Figure 11. Histology of the alibasisphenoidal synchondrosis (abs) in a perinatal *Saimiri boliviensis*, shown in coronal sections. A–C) anterior to posterior sections, showing that the abs connects to the alisphenoid (alis) anteriorly (A), and to the basitrabecular process (btp) of the basisphenoid (bs) posteriorly (C). D–F) Reconstruction of the same stillborn *Saimiri boliviensis* based on aligned CT and histology slices. D) Sphenoid shown in dorsal view with the cartilaginous abs shown in red. The white dashed lines indicate the levels of section A and C. E) Magnification of the same view, with the path of the maxillary (V2) and Vidian nerve (Vn) indicated by green dashed lines. F) Sphenoid, in anterior view, shows all three major trigeminal nerve branches and the course of each nerve passing through its respective foramina. Further abbreviations: cat, cartilage of auditory tube; fo, foramen ovale; os, orbitosphenoid; fr, foramen rotundum. oc, orbital canal; ps, presphenoid; iss, intrasphenoid synchondrosis; sof, superior orbital fissure; V1, ophthalmic division of trigeminal nerve; V3, mandibular divisions of trigeminal nerve. Scale bars: A–C, 0.5 mm; D, 1 mm; E, F, 1.5 mm.

The fate of the chondrocranium is complex, with much of it undergoing endochondral ossification, some parts remaining cartilaginous, some parts resorbing, and some parts undergoing breakdown of cartilaginous matrix (Maier 2000; Smith et al. 2008, 2012, 2021b; Ruf 2020). By far, chondrocranial elements that ossify as elements of the basicranial region of the postnatal skull have received the greatest attention in the literature (e.g., Kodama 1986a, b). In contrast, far fewer studies have examined morphogenesis of chondrocranial bones in multiple stages of development that span pre- and early postnatal life (but see Maier 1987; Zeller 1987). Herein, we have

examined fetal, perinatal, and early postnatal morphogenesis of the sphenoid in a mixed sample of non-human primates, a time period that is notably understudied (Maier 2020b). Though we were unable to examine parallel stages in all species, most of the primates studied here are described for the first time. These data place the human sphenoid in a better comparative perspective.

Table 4. Metrics of the sphenoid expressed as ratios in *Lemur catta* and *Saguinus* spp. across age

	ISS/SL	PS length/width 1	PS length/width 2	BS length/width 1	BS length/width 2
<i>Lemur catta</i>					
fetal	0.186	1.112	0.756	0.814	0.806
newborn	0.133	1.385	1.142	1.385	1.150
one month	0.080	2.213	1.437	1.501	1.323
<i>Saguinus geoffroyi</i>					
fetal	0.410	1.191	1.289	1.146	0.944
newborn	0.068	8.348	2.973	1.832	1.306
<i>Saguinus oedipus</i>					
newborn	0.080	5.601	2.661	1.712	1.394
one month	0.037	6.283	2.751	1.815	1.602

BS length/ width 1: ratio at anterior and of basisphenoid body; BS length/ width 2: ratio at posterior and of basisphenoid body; ISS/SL: ratio of intrasphenoidal synchondrosis to total sphenoid length (= anterior end of presphenoid body to poster end of basisphenoid body); PS length/ width 1: ratio at anterior and of presphenoid body; PS length/ width 2: ratio at posterior and of presphenoid body; SL, total sphenoid length.

Early to mid-fetal morphogenesis of the sphenoid in primates

The most detailed report on sphenoid development in a non-human primate focused on *Loris tardigradus* (Ramaswami 1957). Earlier stages of development have been described in *Galago senegalensis* (Kanagasuntheram and Kanan 1964), but these stages precede ossification. Likewise, embryonic stages of cranial development are well described in some Old World monkeys (e.g., Hendrickx 1971), but later (fetal) stages that reveal patterns of ossification have been virtually ignored in the literature.

In *Loris tardigradus*, the basisphenoid ossifies prior to the presphenoid, as in humans. There is a single center described for the BS body, and paired alar centers. As in humans, the posterior crus of the orbitosphenoid and presphenoid body appear as separate centers and fuse; the anterior crus fuses later (Ramaswami 1957). From our observations, we can confirm that the presphenoid and orbitosphenoid have independent ossification centers in *Saguinus geoffroyi*, and it is most certainly the posterior crus of the latter which ossifies earliest (Fig. 5C). This may indicate a common pattern among primates, as we now have examples in both suborders. However, Maier (2000) interpreted that the presphenoid bone of papionins may form by spreading from the orbitosphenoid and into the presphenoid body. Thus, more studies may be required to establish the degree of variation in how ossification centers emerge.

Our sectioned *Loris tardigradus* specimen establishes that the membranous portion of the bone initiates ossification as a perichondrial extension of the incipient ABS (Fig. 2C), which develops within the alar process of the ala temporalis. This mode of enlargement is already well known based on Maier's (1987) study of *Monodelphis*. The *Loris* fetus also reveals that endochondral growth of the alisphenoid begins at the medial side of the ABS, where it connects to the basitrabecular process of the basisphenoid. This assumes the slender loris goes on to form a bipolar organization of the ABS, as seen in all other primates described here and previously (Smith et al. 2021a).

Regarding the sequence of fusion of portions of the sphenoid, all species fuse the presphenoid/orbitosphenoid complex prior to the basisphenoid and alisphenoid. The former pair may fuse closer to mid gestation, whereas the ABS persists in later fetal (e.g., Fig. 3B), or at least to perinatal age. After the four parts of the sphenoid have formed, the sphenoid participates in at least five active growth centers, the SOS, ISS, PSept, and ABS (paired). We have too few specimens to quantify prenatal changes in synchondroseal growth. But our qualitative and immunohistochemical observations imply that proliferation of chondrocytes in all of these synchondroses is likely very rapid prenatally. In the earliest stage fetus we studied (fetal *Saguinus geoffroyi*), the numerous rows of proliferating and hypertrophic chondrocytes and widespread PCNA activity are impressive compared to newborns. This likely reflects the rapid establishment of pre- and basisphenoid bodies, as well as midline growth of the entire cranium. In midline synchondroses, PCNA activity remains ubiquitous in the proliferating zone at birth, but becomes more restricted in the hypertrophic zone. The implied age-related reduction in mitosis is also characteristic of rodents (Dai et al. 2017). Our report adds some new depth to our understanding of the ABS, which has rarely been discussed comparatively, although it has long been known to exist where the basitrabecular process of the alisphenoid meets the alisphenoid (see Maier 1987, and references therein for further discussion). The reason for this may be its comparatively small size, which means it appears in only a small space even among serial sections, and thus visualization is difficult. However, it has been clearly pictured by authors such as Spatz (1964) who revealed that in the tree shrew (*Tupaia glis*), it appears as a transversely oriented bar connecting the basi- and alisphenoids (fig. 23, therein). In addition, the synchondrosis is clearly indicated as a transverse connection between these two parts of the sphenoid in mice (*Mus musculus*) by McBratney-Owen et al. 2008, see fig. 9B, therein). Thus, in a rodent, a scandentian, most strepsirrhines we studied here (e.g., Figs 3C, 8) the ABS, and its growth potential, is directed primarily in a lateral

direction. Moreover, it is more lateral in mid-fetal than perinatal *Saguinus Geoffroyi* (Fig. 6). In light of this, it appears to be the case that a lateral orientation of the ABS is primitive for eurchontoglires.

Maier (1993) discusses the ontogenetic shift of the site of ABS prenatally. It begins as a cleft between the hypophyseal plate (which gives rise to the basisphenoid) and the ala temporalis (forms the base of the alisphenoid). Later it forms a synchondrosis between these cartilages and then transitions to a suture. Maier (1993) refers to the site as the “*junctura basopalatini*” after Gaupp (1910, cited therein), but notes that it has not been given an official anatomical name (we have suggested alibasisphenoidal synchondrosis or suture for its later stages). Based on Maier’s illustration of the chondrocranium of a marsupial (*Monodelphis*) the joint (1987, fig. 3) is laterally and slightly anteriorly oriented. This could indicate that a lateral orientation is plesiomorphic for all therians.

Monkeys, in contrast including the platyrrhines described here as well as at least one catarrhine (*Papio anubis*) have an ABS that is directed more anteriorly and inferiorly from the basisphenoid. Further observations are clearly needed to assess the broader therian pattern on the one hand, and on the other hand whether all of Anthropoidea are similar in a derived anteroinferiorly directed ABS. Here we also confirm the ABS bears characteristics of an active growth center at fetal stages, including well-organized proliferating and hypertrophic chondrocytes, and PCNA reactivity indicating ongoing mitoses, as discussed more fully below.

Fetal and early postnatal growth of the sphenoid in primates

Although the late fetal *Lemur catta* of known age is only estimated to be ~2 weeks premature (see above) by comparison to average newborn cranial length, a 24% increase is indicated (Table 3). The same age comparison suggests a modest decrease in ISS diameter, and that the sphenoid length increases in tandem with skull length (26%, Table 3). A comparison of infants to newborns suggests the sphenoid may grow more rapidly than the skull as a whole during infancy, and the ISS diminishes (~20%) during this interval (Table 3). The disparity of the presphenoid and basisphenoid length between age groups is not as stark as in the *Saguinus* comparisons (Table 3; also see Fig. 7 regarding proportional changes).

Fetal and newborn *Saguinus Geoffroyi* are markedly different in cranial length (Table 2). Cranial length differs between the fetus and average newborn cranial length by 64% (Table 3). A comparison of ISS diameter reveals a 65% decrease suggesting this synchondrosis may be adding bone to adjacent surfaces of the basisphenoid and presphenoid rapidly during fetal growth. However, the sphenoid differs by 112% in length, suggesting other sphenoidal synchondroses lead to non-isometric growth. This is supported by percentage increase in presphenoid length (361%), which far exceeds that of the basisphenoid, which differs by ~100% in length between the fetus

and newborn (Table 3). Assuming the fetal specimen is typical for its stage, these differences suggest the presphenoid outpaces the basisphenoid in fetal longitudinal growth, and that of cranial length. This certainly agrees with qualitative impressions (Fig. 5), and observations that the anterior limit of the presphenoid projects within the midface at birth (Smith et al. 2017). A comparison of the average cranial and sphenoid dimensions in newborns compared to a single one-month-old suggests a more modest pace of growth during early infancy. If the one-month-old is typical for its age, our findings suggest a modest change (~6%) in cranial length during the first month. But again, the sphenoid, and especially the presphenoid, are outpacing growth of the cranium as a whole (Table 3; 34% increase in presphenoid length, versus 6% for the cranial length).

Our analyses suggest the sphenoid bones have differing midline growth trajectories in platyrrhines and strepsirrhines. Newborn platyrrhines have proportionally longer presphenoids than basisphenoids and our measurements hint that this manifests prenatally, because it is rostrally projected toward the septal cartilage at birth. Proportionally large presphenoids also typify Old World monkeys (Smith et al. 2021a) and this suggests that in monkeys growth in this bone occurs at a faster rate than other sphenoid parts, perhaps especially at the rostral end. Although this may seem counterintuitive in light of limited facial projection in most monkeys, endochondral growth is also redirected more inferiorly in monkeys (Smith et al. 2017, 2021a). Strepsirrhines, by comparison, have a sphenoid growth pattern that is closer to isometric within (i.e., basis-versus presphenoid) and relative to the skull. This may also mean that interstitial chondral growth, as opposed to that which occurs during endochondral ossification, contributes greatly to length increase in the septal cartilage of the strepsirrhines. Similarly, Wealthall and Herring (2006) clearly showed that proliferating chondrocytes of PSept were insufficient to fully explain septal cartilage growth in mice, and that interstitial chondral growth throughout the entire septum explained the remaining growth.

Another synchondroseal growth pattern that differs between strepsirrhines and monkeys occurs at the ABS. Here, we confirm our previous observations (Smith et al. 2021a) that organization of chondrocyte columns in ABS is directionally different in these primate groups, being relatively more laterally directed in strepsirrhines and more anteriorly directed in monkeys. Yet, the findings herein suggest the most significant timeframe in which the ABS might affect the middle cranial fossa occurs prenatally. PCNA reactivity supports a hypothesis that it is active in fetal specimens, and may be present but quiescent or with limited growth potential at birth. However, the evidence also confirms the synchondrosis is greatly diminished in dimensions by the perinatal age, with reduced PCNA reactivity. Therefore, we postulate its primary importance as an active growth center is prenatal. A subtle but notable difference exists between fetal and newborn *Saguinus*. The ABS is directed more laterally in the fetus than in the newborn. In newborns, the ABS is directed both anteriorly and ventrally. The same trajec-

tory is seen in the ABS of newborn *Saimiri*, described above, and in *Papio* (Smith et al. 2021a). This may signify a redirection of interstitial growth late in ontogeny. As this site has been studied little, future work must consider whether important growth events occurring in the middle cranial base affect overall form, as suggested recently by Bastir and Rosas (2006). The implied inferior redirection of the ABS coincides with the same altered trajectory at PSept: initially it orients anteriorly, but in newborns PSept is inclined downward. One possible role of ABS is to ensure the alisphenoid coordinates with downward facial orientation in anthropoids, which is critical because the sphenoid is a key interface between the developing facial skeleton and cranial vault.

The bilateral elements of the sphenoid rely more on appositional bone growth. We should note this begins even prior to endochondral ossification of the ala temporalis in *Loris tardigradus*. The alisphenoid expands within perichondrium of the unossified tip of the ala, with appositional bone extending laterally in the form of a thin plate. This phenomenon was described in detail also in *Monodelphis domestica* by Maier (1987; termed *Zuwachsknochen*). In *Lemur*, the orbitosphenoid ossifies before birth. Thus, perinatal expansion of the orbitosphenoid, like the alisphenoid, is entirely via appositional expansion. Our older infant samples show this continues, and may accelerate, during early infancy.

Conclusion: Implications of comparative sphenoid ontogeny in primates

Non-human primate tissue samples are exceedingly rare due to the slow rate of reproduction and/or conservation status of many species (Smith et al. 2020). Thus, most findings of the present study should be considered as preliminary based on our limited sampling. However, these observations provide a first opportunity to assess in what manner human basicranial development is distinct from other primates in the perinatal timeframe.

Previous studies have now histologically established at least two synchondroses (SOS and ISS) are present in most groups of primates at birth and even at older sub-adult ages (Michejda 1972; Heinkele et al. 1989; Smith et al. 2021a). Now multiple studies have established that the SOS in humans and Old World monkeys has the characteristics of a growth center, including columnar organization of proliferating and hypertrophic chondrocytes; this is most evident early in postnatal life, and then gradually recedes (Thilander and Ingervall 1973; Heinkele et al. 1989). Our descriptive findings and preliminary PCNA data suggest this may be a trend that typifies other primates as well. With a broader perspective across primates, we now see that there are multiple synchondroses requiring further study. At present we consider the PSept and ABS to be distinctively oriented in monkeys (see also

Smith et al. 2021a), which may relate to downward facial orientation.

A particular commonality among anthropoids appears to be the shape of the presphenoid, which becomes disproportionately taller compared to the basisphenoid (Jeffery and Spoor 2002). This begins to manifest during the second trimester in humans. All studied anthropoids exhibit this pattern by birth (Smith et al. 2017, 2021a). But our fetal *Saguinus* suggests tamarins are markedly slower to heighten the presphenoid. As sphenoid height correlates with midfacial growth (Jeffery and Spoor 2002); this may relate to their relatively diminutive midface at birth.

In a broad sense, primates have an accelerated loss of anterior parts of the chondrocranium, such as the posterior nasal cupula (Smith et al. 2021b). In contrast, this part of the capsule remains cartilaginous at birth in *Colugo cynocephalus*, *Tupaia belangeri*, *Rousettus leschenaultia* (all studied in Smith et al. 2017) and in murid rodents (Ruf 2020). This means that the formation of sutural interfaces on the cranial base and face are formed ontogenetically earlier in primates than in many other mammals. Early fusion of ISS in humans may be another example of accelerated development of the anterior part of the chondrocranium. This joint is considered an important site in reference to basicranial flexion by some authors (e.g., Scott 1953; Jeffery and Spoor 2002). An unanswered question remains whether other hominoids resemble humans in early fusion at this site. We should also consider whether the patterns of sphenoid growth shown here for platyrrhines are a more widespread *anthropoid* pattern (i.e., all monkeys, apes, and humans). Certain descriptions of human development indicate this may not be the case at all. For example, all observations to date indicate that the ISS fuses relatively early in humans (Baume 1968; Shopfner et al. 1968; Bosma 1986), and Smith et al. (2017) suggest this may also be true in other hominoids. Further, in newborn humans Baume (1968) described PSept to be in a state of degeneration. Thus, endochondral growth of the sphenoid may play a far more prolonged and significant role in monkeys compared to apes and humans. Conversely, humans, and perhaps hominids generally, may have an accelerated development of the sphenoid in which ISS and PSept cease active growth prenatally. Acceleration of ISS fusion in humans was also suggested by Jeffery and Spoor (2002) as a possible explanation for prenatal changes in basicranial angle.

There remains a critical need to parse out to what extent endochondral bone growth affects basicranial growth and angulation, as well as midfacial projection/orientation, in monkeys versus hominoids. Our ongoing focus is to determine how long various synchondroses remain active, and to assess longer term postnatal trends in development of the sphenoid bone in non-human primates.

Acknowledgements

This is DLC publication # 1482. We thank Gabriel Hughes for his participation in cross-sectional age comparisons of *Otolemur crassicaudatus*. We are also grateful to Irina Ruf and Thomas E. Macrini for thorough and constructive reviews, and to Irina Ruf for editorial corrections.

Funding: NSF; grant numbers BCS-1830894, BCS-1830919, BCS-1231717, BCS-1231350, BCS-1728263; BCS-0959438.

References

- Bastir M, Rosas A (2006) Correlated variation between the lateral basicranium and the face: A geometric morphometric study in different human groups. *Archives of Oral Biology* 51: 814–824. <https://doi.org/10.1016/j.archoralbio.2006.03.009>
- Baume LJ (1968) Patterns of cephalofacial growth and development. A comparative study of the basicranial growth centers in rat and man. *International Dental Journal* 13: 489–513.
- Bosma JF (1986) *Anatomy of the Infant Head*. Johns Hopkins University Press, Baltimore, 488 pp.
- Cendekiawan T, Wong RWK, Rabie ABM (2010) Relationships between cranial base synchondroses and craniofacial development: a review. *The Open Anatomy Journal* 2: 67–75. <https://doi.org/10.2174/1877609401002010067>
- Cunningham C, Scheuer L, Black S (2016) *Developmental Juvenile Osteology*. Academic Press, New York, 630 pp.
- Dai J, Lin, Y, Ningjuan O, Shi J, Yu D, Shen G (2017) Postnatal development of the speno-occipital synchondrosis: A histological analysis. *Journal of Craniofacial Surgery* 28: 1635–1637. <https://doi.org/10.1097/SCS.00000000000003913>
- de Beer GR (1929) The development of the skull of the shrew. *Philosophical Transactions of the Royal Society B* 217: 411–480.
- de Beer GR (1937) *The development of the vertebrate skull*. Chicago University Press, Chicago, 554 pp.
- DeLeon VB, Smith TD (2014) Mapping the nasal airways: using histology to enhance CT-based three-dimensional reconstruction in *Nycticebus*. *Anatomical Record* 297: 2113–2120. <https://doi.org/10.1002/ar.23028>
- Durham E, Howie RN, Parsons T, Bennfors G, Black L, Weinberg SM, Elsalanty M, Yu JC, Cray JJ (2017) Thyroxine exposure effects on the cranial base. *Calcified Tissue International* 101: 300–311. <https://doi.org/10.1007/s00223-017-0278-z>
- Fawcett E (1910) Notes on the development of the human sphenoid. *Journal of Anatomy and Physiology* 44: 207–222.
- Ford EHR (1958) Growth of the human cranial base. *The American Journal of Orthodontics and Dentofacial Orthopedics* 44: 498–506. [https://doi.org/10.1016/0002-9416\(58\)90082-4](https://doi.org/10.1016/0002-9416(58)90082-4)
- Fulwood EL, Boyer DM, Kay RF (2016) Stem members of Platyrrhini are distinct from catarrhines in at least one derived cranial feature. *Journal of Human Evolution* 100: 16–24. <https://doi.org/10.1016/j.jhevol.2016.08.001>
- Heinkele M, Freiburg R, Ewers K (1989) Die Synchondrosis sphenoo-cipitalis—Eine fluoreszenz- und polarisationsmikroskopische Untersuchung am *Cercopithecus-aethiops*-Affen. *Fortschritte der Kieferorthopädie* 50: 493–505.
- Hendrickx AG (1971) *Embryology of the Baboon*. University of Chicago Press, Chicago, 205 pp.
- Hoyte DAN (1973) Basicranial elongation: 2. Is there differential growth within a synchondrosis? *Anatomical Record* 175: 347.
- Hunziker EB (1994) Mechanism of longitudinal bone growth and its regulation by growth plate chondrocytes. *Microscopy Research and Technique* 28: 505–519. <https://doi.org/10.1002/jemt.1070280606>
- Jeffery N, Spoor F (2002) Brain size and the human cranial base: A prenatal perspective. *American Journal of Physical Anthropology* 118: 324–340. <https://doi.org/10.1002/ajpa.10040>
- Kanagasuntheram R, Kanan CV (1964) The chondrocranium of a 19 mm C.R. length embryo of *Galago senegalensis*. *Acta Zoologica* 45: 107–121.
- Kawasaki K, Richtsmeier JT (2017) Association of the chondrocranium and dermatocranium in early skull formation. In: Percival CJ, Richtsmeier JT (Eds) *Building Bones: Bone Formation and Development in Anthropology*. Cambridge University Press, Cambridge, 52–78. <https://doi.org/10.1017/9781316388907.004>
- Kier EL, Rothman LG (1986) Radiologically significant anatomic variations of the development sphenoid in humans. In: Bosma JF (Ed) *Development of the Basicranium*. DHEW Publication No. (NIH) 76–989. National Institutes of Health, Bethesda MD, 107–140.
- Kjaer I (1990) Ossification of the human fetal basicranium. *Journal of Craniofacial Genetics and Developmental Biology* 10: 29–38.
- Kodama G (1986a) Developmental studies on the presphenoid of the human sphenoid bone. In: Bosma JF (Ed) *Development of the basicranium*. DHEW Publication No. (NIH) 76–989. National Institutes of Health, Bethesda MD, 141–155.
- Kodama G (1986b) Developmental studies on the body of the human sphenoid bone. In: Bosma JF (Ed) *Development of the basicranium*. DHEW Publication No. (NIH) 76–989. National Institutes of Health, Bethesda MD, 156–165.
- Krieborg S, Marsh JL, Cohen MM Jr, Liversage M, Pedersen H, Skovby F, Borgeesen SE, Vannier MW (1993) Comparative three-dimensional analysis of CT-scans of the calvaria and cranial base in Apert and Crouzon syndromes. *Journal of Cranio-Maxillofacial Surgery* 21: 181–188. [https://doi.org/10.1016/S1010-5182\(05\)80478-0](https://doi.org/10.1016/S1010-5182(05)80478-0)
- Lesciotto KM, Richtsmeier JT (2019) Craniofacial skeletal response to encephalization: How do we know what we think we know? *Yearbook of Physical Anthropology* 168: 27–46. <https://doi.org/10.1002/ajpa.23766>
- Lieberman DE, Ross CF, Ravosa MJ (2000) The primate cranial base: ontogeny, function, and integration. *Yearbook of Physical Anthropology* 43: 117–169. [https://doi.org/10.1002/1096-8644\(2000\)43:31-+<117::AID-AJPA5>3.0.CO;2-I](https://doi.org/10.1002/1096-8644(2000)43:31-+<117::AID-AJPA5>3.0.CO;2-I)
- Maier W (1983) Morphology of the interorbital region of *Saimiri sciureus*. *Folia Primatologica* 41: 277–303. <https://doi.org/10.1159/000156137>
- Maier W (1987) The ontogenetic development of the orbitotemporal region in the skull of *Monodelphis domestica* (Didelphidae, Marsupialia), and the problem of the mammalian alisphenoid. In: Kuhn H-J, Zeller U (Eds) *Morphogenesis of the Mammalian Skull (Mammalia depicta 13)*. Paul Parey, Hamburg, 71–90.
- Maier W (1993) Cranial morphology of the therian common ancestor, as suggested by the adaptations of neonate marsupials. In: Szalay FS, Novacek MJ, McKenna MC (Eds) *Mammal Phylogeny*. Springer, New York, 165–181.
- Maier W (2000) Ontogeny of the nasal capsule in cercopithecoids: a contribution to the comparative and evolutionary morphology of catarrhines. In: Whitehead PF, Jolly C (Eds) *Old World Monkeys*. Cambridge University Press, Cambridge, 99–132.

- Maier W (2020a) A neglected part of the mammalian skull: The outer nasal cartilages as progressive remnants of the chondrocranium. *Vertebrate Zoology* 70: 367–382. <https://doi.org/10.26049/VZ70-3-2020-09>
- Maier W (2020b) Foreword. Perinatal anatomy of primates – a neglected ontogenetic stage. In: Smith TS, DeLeon VB, Vinyard CJ, Young JW (Authors) *Skeletal Anatomy of the Newborn Primate*. Cambridge University Press, Cambridge, vii–xi.
- McBratney-Owen B, Iseki S, Bamforth SD, Olsen BR, Morris-Kay GM (2008) Development and tissue origins of the mammalian cranial base. *Developmental Biology* 322: 121–132. <https://doi.org/10.1016/j.ydbio.2008.07.016>
- Michejda M (1972) The role of basicranial synchondroses in flexure processes and ontogenetic development of the skull base. *American Journal of Physical Anthropology* 37: 143–150. <https://doi.org/10.1002/ajpa.1330370119>
- Melsen B (1974) The cranial base: The postnatal development of the cranial base studied histologically on human autopsy material. *Acta Odontologica Scandinavica* 32: 9–126.
- Melsen B (1977) Histological analysis of the postnatal development of the nasal septum. *The Angle Orthodontist* 47: 83–96. [https://doi.org/10.1043/0003-3219\(1977\)047<0083:HAOTPD>2.0.CO;2](https://doi.org/10.1043/0003-3219(1977)047<0083:HAOTPD>2.0.CO;2)
- Moore RN (1978) A cephalometric and histologic study of the cranial base in foetal monkeys, *Macaca nemestrina*. *Archives of Oral Biology* 23: 57–67. [https://doi.org/10.1016/0003-9969\(78\)90141-3](https://doi.org/10.1016/0003-9969(78)90141-3)
- Pitirri MK, Kawasaki K, Richtsmeier JT (2020) It takes two: Building the vertebrate skull from chondrocranium and dermatocranium. *Vertebrate Zoology* 70: 587–600. <https://doi.org/10.26049/VZ70-4-2020-04>
- Presley R (1993) Preconception of adult structural pattern in the analysis of the developing skull. In: Hanken JH, Hall BK (Eds) *The skull*. Vol. 1. Development. University of Chicago Press, Chicago, 347–377
- Ramaswami LS (1957) The development of the skull in the slender loris, *Loris tardigradus lydekkerianus* Cabr. *Acta Zoologica* 38: 27–68. <https://doi.org/10.1111/j.1463-6395.1957.tb00050.x>
- Ruf I (2020) Ontogenetic transformations of the ethmoidal region in Muroidea (Rodentia, Mammalia): new insights from perinatal stages. *Vertebrate Zoology* 70: 383–415. <https://doi.org/10.26049/VZ70-3-2020-10>
- Sánchez-Villagra MR, Forasiepi AM (2017) On the development of the chondrocranium and the histological anatomy of the head in perinatal stages of marsupial mammals. *Zoological Letters* 3:1. <https://doi.org/10.1186/s40851-017-0062-y>
- Sasaki H, Kodama G (1986) Developmental studies of the postsphenoid of the human sphenoid bone. In: Bosma JF (Ed) *Development of the basicranium*. DHEW Publication No. (NIH) 76-989. National Institutes of Health, Bethesda MD, 177–191.
- Schunke AC, Zeller U (2010) Chondrocranium and dermal bones of the Lowland Streaked Tenrec *Hemicentetes semispinosus* (Afrosoricida, Tenrecidae) and their comparison with *Potamogale* and other insectivoran-grade placental mammals. *Vertebrate Zoology* 60: 37–72.
- Scott JH (1953) The cartilage of the nasal septum. *British Dental Journal* 95: 37–43.
- Scott JH (1958) The cranial base. *American Journal of Physical Anthropology* 16: 319–348. <https://doi.org/10.1002/ajpa.1330160305>
- Shopfner CE, Wolfe TW, O’Kell RT (1968) The intersphenoid synchondrosis. *American Journal of Roentgenology* 104: 184–193.
- Smith TD, Rossie JB, Docherty BA, Cooper GM, Bonar CJ, Silverio AL, Burrows AM (2008) Fate of the nasal capsular cartilages in pre-natal and perinatal tamarins (*Saguinus Geoffroyi*) and extent of secondary pneumatization of maxillary and frontal sinuses. *The Anatomical Record* 291: 1397–1413. <https://doi.org/10.1002/ar.20787>
- Smith TD, Rossie JB, Cooper GM, Durham EL, Schmeig RM, Docherty BA, Bonar CJ, Burrows AM (2012) Microanatomical variation of the nasal capsular cartilage in newborn primates. *The Anatomical Record* 295: 950–960. <https://doi.org/10.1002/ar.22448>
- Smith TD, Jankord KD, Progar AJ, Bonar CJ, Evans S, Williams L, Vinyard CJ, DeLeon VB (2015) Dental maturation, eruption, and gingival emergence in the upper jaw of newborn primates. *The Anatomical Record* 298: 2098–2131. <https://doi.org/10.1002/ar.23273>
- Smith TD, McMahon MJ, Millen ME, Llera C, Engel SM, Li L, Bhatnagar KP, Burrows AM, Zumpano MP, DeLeon VB (2017) Growth and development at the sphenothmoidal junction in perinatal primates. *The Anatomical Record* 300: 2115–2137. <https://doi.org/10.1002/ar.23630>
- Smith TD, DeLeon VB, Vinyard CJ, Young JW (2020) *Skeletal anatomy of the newborn primate*. Cambridge University Press, Cambridge, 328 pp.
- Smith TD, Reynolds RL, Mano N, Wood BJ, Oladipupo L, Corbin HM, Taylor J, Ufelle A, Burrows AM, Durham E, Vinyard CJ, Cray JJ, DeLeon VB. (2021a) Cranial synchondroses in primates at birth. *The Anatomical Record* 304: 1020–1053. <https://doi.org/10.1002/ar.24521>
- Smith TD, Ufelle AC, Cray JJ, Rehorek SB, DeLeon VB (2021b) Inward collapse of the nasal cavity: Perinatal consolidation of the midface and cranial base in primates. *The Anatomical Record* 304: 939–957. <https://doi.org/10.1002/ar.24537>
- Som PM, Naidich TP (2013) Development of the skull base and calvarium: an overview of the progression from mesenchyme to chondrification to ossification. *Neurographics* 3: 169–184. <https://doi.org/10.3174/ng.4130069>
- Spatz W (1964) Beitrag zur Kenntnis der Ontogenese des Cranium von *Tupaia glis* (Diard, 1820). *Gegenbaurs Morphologisches Jahrbuch* 106: 321–416.
- Sperber GH (2001) *Craniofacial Development*. BC Decker, Hamilton, 220 pp.
- Starck, D (1967) Le crâne des mammifères. In: Grassé P-P (Ed) *Traité de Zoologie*, XVI. Masson, Paris, 405–549.
- Starck D (1975) The development of the chondrocranium in primates. In: Luckett WP, Szalay FS (Eds) *Phylogeny of the Primates*. Plenum Press, New York, 127–155.
- Thilander B, Ingervall B (1973) The human sphenoccipital synchondrosis II. A histological and microradiographic study of its growth. *Acta Odontologica Scandinavica* 31: 323–336. <https://doi.org/10.3109/00016357309002520>
- Wealthall RJ, Herring SW (2006) Endochondral ossification of the mouse nasal septum. *The Anatomical Record* 288A: 1163–1172. <https://doi.org/10.1002/ar.a.20385>
- Werneburg I (2020) Editorial to the special issue (virtual issue) 2019/2020 Recent Advances in Chondrocranium Research. *Vertebrate Zoology* 69/70: I–VIII. <https://doi.org/10.26049/VZ-69-70-Special-Issue>
- Yamamoto M, Cho KH, Murakami G, Abe S, Rodríguez-Vázquez JF (2018) Early fetal development of the otic and pterygopalatine ganglia with special reference to the topographical relationship with the developing sphenoid bone. *The Anatomical Record* 301: 1442–1453. <https://doi.org/10.1002/ar.23833>
- Yoon T-M, Park SH, Kwon M, Lee K-J (2019) Immunohistochemical study on the postnatal growth changes of the sphenoccipital

synchondrosis and tibial cartilage. *APOS Trends in Orthodontics* 9: 149–155. https://doi.org/10.25259/APOS_70_2019

Zeller U (1987) Morphogenesis of the mammalian skull with special reference to *Tupaia*. In: Kuhn H-J, Zeller U (Eds) Morphogenesis of the Mammalian Skull (*Mammalia depicta* 13). Paul Parey, Hamburg, 17–50.

Supplementary material 1

***Saguinus oedipus*: Negative control slides for immunohistochemistry.**

Authors: Mano N, Wood B, Oladipupo L, Reynolds R, Taylor J, Durham E, Cray JJ, Vinyard C, DeLeon VB, Smith TD (2021)

Data type: .jpg

Explanation note: Figure S1. Sections from newborn *Saguinus oedipus* prepared for PCNA immunohistochemistry, with fast green counterstain. A sphenoccipital synchondrosis (sos) showing numerous dark-brown stained chondrocytes; B) nearby section of same specimen with primary antibody omitted. C) growth center in cervical vertebra showing numerous dark-brown stained chondrocytes; D) nearby section of same specimen with primary antibody omitted. Scale bars: A, 50 μm ; B–D, 20 μm .

Copyright notice: This dataset is made available under the Open Database License (<http://opendatacommons.org/licenses/odbl/1.0>). The Open Database License (ODbL) is a license agreement intended to allow users to freely share, modify, and use this Dataset while maintaining this same freedom for others, provided that the original source and author(s) are credited.

Link: <https://doi.org/10.3897/vz.71.e65934.suppl1>

Supplementary material 2

***Varecia variegata*: Negative control slides for immunohistochemistry.**

Authors: Mano N, Wood B, Oladipupo L, Reynolds R, Taylor J, Durham E, Cray JJ, Vinyard C, DeLeon VB, Smith TD (2021)

Data type: .jpg

Explanation note: Figure S2. Sections from newborn *Varecia variegata* prepared for PCNA immunohistochemistry, with no counterstain. A) sphenoccipital synchondrosis (sos) showing numerous chondrocytes that are lightly-stained brown; B) nearby section of same specimen with primary antibody omitted, showing no background staining of chondrocytes. Scale bars: 20 μm .

Copyright notice: This dataset is made available under the Open Database License (<http://opendatacommons.org/licenses/odbl/1.0>). The Open Database License (ODbL) is a license agreement intended to allow users to freely share, modify, and use this Dataset while maintaining this same freedom for others, provided that the original source and author(s) are credited.

Link: <https://doi.org/10.3897/vz.71.e65934.suppl2>

Supplementary material 3

***Saguinus geoffroyi* fetus: two sectional planes of alibasisphenoidal synchondrosis.**

Authors: Mano N, Wood B, Oladipupo L, Reynolds R, Taylor J, Durham E, Cray JJ, Vinyard C, DeLeon VB, Smith TD (2021)

Data type: .jpg

Explanation note: **Figure S3.** Three-dimensional reconstruction of the sphenoid bone in fetal *Saguinus geoffroyi* in endocranial view against ghosted skull. A) Dashed lines indicate coronal and sagittal planes through the alibasisphenoidal synchondrosis (abs). These approximate the histological sections made of two halves of the head in coronal (B) and sagittal (C) planes, respectively. Further abbreviations: alis, alisphenoid; at, auditory tube; bo, basioccipital; bs, basisphenoid; btp, basitrabecular process; ps, presphenoid; Vn, Vidian nerve. Scale bars: A, 1 mm, B, 100 µm; C, 250 µm.

Copyright notice: This dataset is made available under the Open Database License (<http://opendatacommons.org/licenses/odbl/1.0>). The Open Database License (ODbL) is a license agreement intended to allow users to freely share, modify, and use this Dataset while maintaining this same freedom for others, provided that the original source and author(s) are credited.

Link: <https://doi.org/10.3897/vz.71.e65934.suppl3>

Supplementary material 4

***Otolemur crassicaudatus*: age-changes in patency of alibasisphenoidal synchondrosis.**

Authors: Mano N, Wood B, Oladipupo L, Reynolds R, Taylor J, Durham E, Cray JJ, Vinyard C, DeLeon VB, Smith TD (2021)

Data type: .jpg

Explanation note: **Figure S4.** Late fetal (A, B) and one-month-old (C) specimens of *Otolemur crassicaudatus*, showing the alibasisphenoidal synchondrosis (*) at two ages. Note the marked reduction in the mediolateral breadth of the joint between the perinatal and infant stages. Further abbreviations: alis, alisphenoid; bs, basisphenoid; btp, basitrabecular process; os, orbitosphenoid; ps, presphenoid. Scale bars: A, 1 mm; B, 0.5 mm; C, 1 mm.

Copyright notice: This dataset is made available under the Open Database License (<http://opendatacommons.org/licenses/odbl/1.0>). The Open Database License (ODbL) is a license agreement intended to allow users to freely share, modify, and use this Dataset while maintaining this same freedom for others, provided that the original source and author(s) are credited.

Link: <https://doi.org/10.3897/vz.71.e65934.suppl4>

Supplementary material 5

Age changes in synchondroses in two primate genera.

Authors: Mano N, Wood B, Oladipupo L, Reynolds R, Taylor J, Durham E, Cray JJ, Vinyard C, DeLeon VB, Smith TD (2021)

Data type: .docx

Explanation note: **Table S1.** Sphenoid measurements (in mm) of subadult Lemur catta and Saguinus spp.

Copyright notice: This dataset is made available under the Open Database License (<http://opendatacommons.org/licenses/odbl/1.0>). The Open Database License (ODbL) is a license agreement intended to allow users to freely share, modify, and use this Dataset while maintaining this same freedom for others, provided that the original source and author(s) are credited.

Link: <https://doi.org/10.3897/vz.71.e65934.suppl5>

Supplementary material 6

Identifying information of specimens examined descriptively.

Authors: Mano N, Wood B, Oladipupo L, Reynolds R, Taylor J, Durham E, Cray JJ, Vinyard C, DeLeon VB, Smith TD (2021)

Data type: .docx

Explanation note: Table S2. Other specimens examined descriptively.

Copyright notice: This dataset is made available under the Open Database License (<http://opendatacommons.org/licenses/odbl/1.0>). The Open Database License (ODbL) is a license agreement intended to allow users to freely share, modify, and use this Dataset while maintaining this same freedom for others, provided that the original source and author(s) are credited.

Link: <https://doi.org/10.3897/vz.71.e65934.suppl6>